Concentrating Solar Power Tower: Latest Status Report and Survey of Development Trends

Albert Boretti [1],*, Stefania Castelletto [2] and Sarim Al-Zubaidy [3]

[1]   Department of Mechanical and Aerospace Engineering (MAE), Benjamin M. Statler College of Engineering and Mineral Resources, West Virginia University, Morgantown, WV 26506, United States, alboretti@mail.wvu.edu; a.a.boretti@gmail.com

[2]   School of Engineering, RMIT University, Bundoora, VIC 3083, Australia; stefania.castelletto@rmit.edu.au

[3]   The University of Trinidad and Tobago, Trinidad and Tobago; president@utt.edu.tt

*   Correspondence: alboretti@mail.wvu.edu; a.a.boretti@gmail.com

Abstract: The paper examines design and operating data of current concentrated solar power (CSP) solar tower (ST) plants. The study includes CSP with or without boost by combustion of natural gas (NG), and with or without thermal energy storage (TES). The latest, actual specific costs per installed capacity are very high, 6085 \$/kW for Ivanpah Solar Electric Generating System (ISEGS) with no TES, and 9227 \$/kW for Crescent Dunes with TES. The actual production of electricity is very low and much less than the expected. The actual capacity factors are 22% for ISEGS, despite combustion of a significant amount of NG largely exceeding the planned values, and 13% for Crescent Dunes. The design values were 33% and 52%. The study then reviews the proposed technology updates to produce better ratio of solar field power to electric power, better capacity factor, better matching of production and demand, lower plant's cost, improved reliability and increased life span of plant's components. The key areas of progress are found in materials and manufacturing processes, design of solar field and receiver, receiver and power block fluids, power cycle parameters, optimal management of daily and seasonal operation of the plant, new TES concepts, integration of solar plant with thermal desalination, integration of solar plant with combined cycle gas turbine (CCGT) installations and finally, specialization and regionalization of the project specification.

Keywords: renewable energy; concentrated solar power; solar tower; parabolic trough; natural gas boost; thermal energy storage; molten salt; steam; Rankine cycles

1. Introduction

The basic principles of concentrated solar power (CSP) systems are covered in previous reference works such as [1], [2], [3], [4] and [5]. Lenses or mirrors concentrate the sun light energy on a small area. The concentrated radiant energy is then converted to heat at high temperature. The heat is finally transferred to a power cycle working fluid (typically water/steam). Superheated steam typically drives a Rankine steam turbine cycle. Concentrators differ in the way they track the sun and focus the light. The most popular concentrating technologies are Parabolic Trough (PT) and Solar Tower (ST). Different concentrators provide different receiver temperature and peak temperature of the steam for the power cycle, with correspondingly varying thermal efficiency of the power cycle. In addition to the type of receiver and the solar field feeding this receiver, also the receiver fluid (RF) plays a role in the peak temperatures of the steam. Current RFs include oil, molten salt (MS) or water/steam. Intermediate heat exchangers are needed between oil or MS and water/steam. MS permits thermal energy storage (TES) in hot and cold reservoir to decouple electricity production from availability of sun light. While an additional MS circuit has been proposed as an appendage to existing CSP plants with oil as RF, MS provides better outcome when used directly as the RF. Replacement of oil with MS permits operation at higher temperatures for

46 higher steam temperature and higher efficiency of power generation. Additionally, it lowers the cost
47 of TES. Direct use of water/steam as a RF has the advantage of simplicity, cost and sometimes
48 efficiency. However, this links the production of electricity to sun availability. Condensation of
49 steam usually occurs in air-cooled towers. Water cooled condensers may permit better power cycle
50 efficiencies but are impractical in mostly desert locations.
51   By using the combustion of natural gas (NG), it is possible to drastically improve the match
52 between production and demand of CSP plants. However, boost by NG is reasonable only if
53 performed in minimal extent, for both efficiency of energy use and regulations concerning emissions
54 of carbon dioxide. The use of NG in a combined cycle gas turbine (CCGT) plant occurs with a fuel
55 conversion efficiency that is about double the efficiency of a CSP plant operated with NG only (η
56 above 60% vs. η around 30%). The spreading in between the η of a CSP plant and a NG fueled plant
57 is similarly large in cases of cogeneration, where the gas turbine (GT) plant also features production
58 of process heat, for heating, cooling, desalination or other activities. Therefore, it is not efficient to
59 design a CSP ST plant requiring a significant NG combustion.
60   The ST technology offers theoretically higher efficiency because of higher temperature.
61 However, the technology is also more demanding from economic and technical view-points. While
62 ST plants are certainly less widespread than PT plants [6], there is an open debate in the literature
63 about which CSP technology may have the better perspectives.
64   The net capacity of Ivanpah Solar Electric Generating System (ISEGS) is 377 MW, while the net
65 capacity of Solar Energy Generating Systems (SEGS) SEGS II-IX is 340 MW. Both facilities use NG to
66 boost the electricity production. ISEGS uses NG in a greater extent than the SEGS facilities. Both
67 ISEGS and SEGS lack of TES. The actual capacity factors (ε) of both installations (electricity produced
68 in a year divided by the product of net capacity by number of hours in a year) is about 20%
69 disregarding the boost by combustion of NG, which is however not negligible as shown in [8] and
70 here further discussed.
71   The global market of CSP is dominated by PT plants, about 90% of all the CSP plants [6]. As per
72 [6], back in 2010 the ST component of CSP was overshadowed by the PT component, accounting for
73 more than 90% of the total CSP installed capacity. The situation has not drastically changed since
74 then [7]. Regardless, the world largest CSP plant, ISEGS uses ST technology. ISEGS is made up of
75 three installations one close to the other. The second largest CSP project in the world, the SEGS
76 facility, is based on PT. This project is made up of 8 different installations presently operational.
77   The CSP technologies presently do not compete on price with photovoltaics (PV) solar panels
78 that have progressed massively in recent years because of the decreasing prices of the PV panels and
79 the much smaller operating costs. While the uptake of solar energy is still minimal, the CSP
80 component is largely overshadowed by the PV component [9]. While CSP may have the potential to
81 play a key role in balancing renewable energy production, the technology is presently living in the
82 shadow of PV [9].
83   Both installed capacity (power) and electricity production (energy) data show the CSP ST
84 technology is overshadowed by the CSP PT technology, while overall the CSP technology suffers
85 from the more competitive costs of PV, while the total solar contribution to the global energy mix is
86 still minimal. [7], [10], [11], [6], [9]. According to [7], in 2016 globally only wind and solar PV power
87 systems have seen a considerable growth in terms of capacity installed compared to 2015 data. In
88 2016 globally the hydropower capacity has been 1,096 GW (in 2015 1,071 GW), the bio-power
89 capacity has been 112 GW (in 2015 106 GW), the geothermal power capacity has been 13.5 GW, (in
90 2015 13 GW), the CSP capacity has been 4.8 GW (in 2015 4.7 GW). Conversely in 2016 the global wind
91 power capacity has been 487 GW, more than 10% higher than the year before (433 GW) and the
92 global solar PV capacity has been 303 GW, almost 40% more than the 2015 value of 228 GW. The
93 installed capacity of CSP is only about 1.5% of the total solar power capacity, where the installed
94 capacity of PV is 98.5% of the total solar power capacity.
95   As explained in Ref. [8], the installed capacity (power) is particularly misleading in case of solar
96 if used to indicate the actual annual production of electricity (energy) by these systems, as the
97 capacity factors (electricity produced divided by the product of the installed capacity by the number

of hours in a year) of recent CSP plants, for example ISEGS [12], [13], [14], [15], are only about 20%, even conceding the benefit of a production boost by combustion of NG.

In terms of energy, according to the International Energy Agency [10], the 2014 World electricity generation has been 23,816 TWh, with Coal/Peat providing the 40.8%, NG the 21.6%, Hydro the 16.4%, Nuclear the 10.6%, Oil the 4.3%, and Others, including all the Renewables the 6.3%. This 6.3% is mostly wind. Presently, the total solar electricity generation in the world is only 1.05% of the total. According to the United States Energy Information Administration [11], the net generation in the United States during 2015 has been 31.2% by coal, 34.7% by NG, 20.2% nuclear, 6.7% by conventional hydroelectric, 5.7% by wind, and 1.4% all solar. As CSP plants only represent 1.5% of the worldwide installed capacity of solar electricity plants, the total CSP contribution to the global energy mix is therefore less than 0.02% [7], [10]. The situation in the United States is not far from the world average. The contribution by CSP ST is then an even smaller 0.0002%.

This scenario is expected to drastically change in the next few years, and there is a clear need to develop new CSP ST technologies to match the significant demand. However, this requires significant technology updates that is unclear could be delivered.

Ref. [16] discusses the most relevant drivers and barriers for the deployment of CSP in the EU by 2030. Apart from supporting policies, the most relevant drivers are the added value of CSP in terms of energy storage that makes them more reliable compared to other renewable energy technologies, and the substantial cost reductions that are expected for the technology. The most relevant barriers are the still very high cost of the technology when compared to conventional power plants and other renewable energy technologies, and the uncertainty of policies. Hence, reduction of costs of the CSP technology is the key factor for a growth. Similarly, Ref. [17] discusses the main reasons why Chinese and Brazilian energy policies so far have not been focused on CSP. As the high Levelized Cost of Electricity (LCOE) of large scale deployment of CSP technologies may affect the competitiveness of national industry in global markets, a comprehensive answer may only follow global policies. CSP has not benefited so far from the global demand that has boosted wind and solar photovoltaic with their subsequent price reductions.

Aims of this paper are to provide an objective assessment of the current costs and performances of CSP ST plants, and then to survey the proposed technologies the many issues that strongly limit the current outlook of CSP ST. As the present costs and performances differ considerably from the planned values, this negatively impacts on the reliability of the figures circulated in the surveyed peer review works.

2. Assessment of present status of CSP ST technology

Concentrating solar power (CSP) has been so far mostly proposed and implemented in the parabolic through (PT) technology. 90% of the CSP plants are indeed PT. Hence, we start this state-of-the-art paragraph with a reference to the PT technology to move then to the ST technology. Incidents and accidents are not considered in the present analysis, similarly to the environmental impacts. The substantial land requirements for CSP are also not included in the analysis.

2.1 List of CSP ST plants

The number of existing CSP ST plants of significant size is very limited, and the time they have been operational is also minimal. Additionally, not all the data needed are publicly available. Hence, the full potential of the ST technology is not shown by the surveys of plants.

In the list of the ST plants of [18], here reproduced as Table 1, there are only 34 CSP ST plants worldwide. Only 3 above 20 MW of capacity are operational, ISEGS of 377 MW capacity since 2014, Crescent Dunes Solar Energy Project (Tonopah) of 110 MW capacity since 2015, and Khi Solar One of 50 MW capacity since 2016. The 377 MW ISEGS plant only producing 703,039 MWh/year (2016), the output of a medium to small scale CCGT plant, has the best data set covering 3 years.

Without a proper, extensive real-world experience, costs, reliability and production data over the plant life span may only be poorly addressed.

147   **Table** 1 – List of solar power tower projects (from [18]).

project	capacity	status	year start
Tamarugal Solar Energy Project	450	under development	
Likana Solar Energy Project	390	under development	
Ivanpah Solar Electric Generating System (ISEGS)	377	operational	2014
Copiapó	260	under development	
Golmud	200	under construction	
Aurora Solar Energy Project	135	under development	
Huanghe Qinghai Delingha 135 MW DSG Tower	135	under development	
NOOR III	134	under construction	
Ashalim Plot B (Megalim)	121	under construction	
Atacama-1	110	under construction	
Crescent Dunes Solar Energy Project (Tonopah)	110	operational	2015
Golden Tower 100MW Molten Salt project	100	under development	
Redstone Solar Thermal Power Plant	100	under development	
SunCan Dunhuang 100 MW Phase II	100	under construction	
Yumen 100MW Molten Salt Tower CSP project	100	under development	
MINOS	52	under development	
Hami 50 MW CSP Project	50	under development	
Khi Solar One	50	operational	2016
Qinghai Gonghe 50 MW CSP Plant	50	under development	
Shangyi 50MW DSG Tower CSP project	50	under development	
Supcon Solar Project	50	under construction	
Yumen 50MW Molten Salt Tower CSP project	50	under construction	
Planta Solar 20 (PS20)	20	operational	2009
Gemasolar Thermosolar Plant (Gemasolar)	19.9	operational	2011
Planta Solar 10 (PS10)	11	operational	2007
SunCan Dunhuang 10 MW Phase I	10	operational	2016
Sierra SunTower (Sierra)	5	operational	2009
Lake Cargelligo	3	operational	2011
ACME Solar Tower	2.5	operational	2011
Jülich Solar Tower	1.5	operational	2008
Sundrop CSP Project	1.5	operational	2016
Jemalong Solar Thermal Station	1.1	operational	2016
Dahan Power Plant	1	operational	2012
Greenway CSP Mersin Tower Plant	1	operational	2012

148   *2.2 Parabolic trough typical design parameters*

149   The most common CSP systems are PT. A PT is made up of a linear parabolic reflector
150   concentrating the sun light onto a tubular receiver. The receiver is located along the focal line of the
151   reflector. The tubular receiver is filled with a working fluid. The RF may be oil, MS or water/steam.
152   The reflectors follow the sun with tracking along a single axis. The working fluid is heated as it flows
153   through the receiver up to temperatures from 390 to 500 °C, depending on the fluid used. If oil or
154   MS, this fluid is then used as the heat driving the production of steam for the power cycle in a heat
155   exchanger. The shaped mirrors of a PT focus the sun light on a tube running along the focus line
156   with an 80 times concentration. The sun light is absorbed by tube that is often in a glass vacuum, and
157   delivered to the RF.

158   PT are in principle less efficient than ST [19], as the temperature of the hot source is typically
159 larger in ST installations, and the efficiency of a Carnot machine is well known to change with the
160 temperature of hot and cold sources as

161
$$\eta = 1 - \frac{T_C}{T_H} \qquad\qquad (1)$$

162 where T_H is the temperature of the hot source and T_C is the temperature of the cold source. They are
163 however much simpler and they are less expensive to build and operate. Hence, the much wider use
164 [6].
165   Reference PT specifications change with the RF and the availability of TES (data from [20], [21],
166 [22], [23], [8], [19]):
167 –   For oil as the RF, the receiver temperature is 390 °C, the peak flux on receiver is about 25 kW/m²,
168   the hot storage temperature is 390 °C, the cold storage temperature is 290 °C, and the condenser
169   temperature for heat rejection is 40 °C.
170 –   For MS (nitrate salt) as the RF, the receiver temperature is 500 °C, the peak flux on receiver is
171   about 25 kW/m², the hot storage temperature is 500 °C, and the cold storage temperature is 300
172   °C.
173 –   In case of water/steam as the RF, the receiver temperature is 500 °C, the peak flux on receiver is
174   about 25 kW /m². There are in this case no hot and cold storage tanks.

175 *2.3 Solar tower typical design parameters*

176   A ST concentrates the sun light from a field of heliostats on a central tower. The heliostats are
177 dual axis tracking reflectors grouped in arrays. They concentrate sunlight on a relatively small
178 central receiver located at the top of the tower. The sun light with ST is much more concentrated
179 than in PT. The RF may be heated to temperatures from 500 to 1000 °C depending on the RFs and the
180 solar concentration design. When MS is used, it serves as the heat driving the production of steam
181 for the power cycle in a heat exchanger. When water/steam is used, then there is no need of this heat
182 exchanger. The field of heliostats focus the light on top of the tower with a 500 to 1000 times
183 concentration. Light is absorbed by metal tubes and delivered to the RF, either water/steam or MS
184 (nitrate salt). Due to sunlight shaded, blocked, absorbed, or spilled, there is a 40% loss of incident
185 light collected by the RF. Receiver, piping, and tank thermal losses further reduced the amount of
186 energy transferred to the power cycle.
187   The reference ST specifications change with the RF and the availability of TES (data from [20],
188 [8], [24], [25]):
189 –   For MS (nitrate salt) as the RF, the receiver temperature is 565 °C, the peak flux on receiver is
190   1,000 kW/m², the hot storage temperature is 565 °C, the cold storage temperature is 290 °C, and
191   the condenser temperature for heat rejection is 40 °C.
192 –   In case of water/steam as the RF, the receiver temperature is 550 °C, the peak flux on receiver is >
193   300 kW/m². The hot and cold storage tanks are not available in this case.

194 *2.4 Additional information of existing plants from thermal models*

195   Computational tools are used for heat balance design of thermal power systems, and for
196 simulation of off-design plant performance. Hence, thermal models are the best avenue to appreciate
197 design variants in CSP ST plants from the point of view of electricity output.
198   A scheme of the Rice CSP ST facility is provided in figure 1 (from [26]). The Rice Solar Energy
199 Project was a latest generation CSP ST project [27] put on hold. The proposed location was Rice,
200 California (Mojave Desert, near Blythe). The gross turbine capacity is 150 MW. The land area is 5.706
201 km². The solar resource is 2,598 kWh/m²/year. The planned electricity generation was 450,000
202 MWh/year. The heliostat solar-field aperture area is 1,071,361 m². The number of heliostats is 17,170,
203 and every heliostat has an aperture area of 62.4 m². The tower height is 164.6 m. The receiver type is
204 external, cylindrical. The heat-transfer fluid is MS. The receiver inlet temperature is 282 °C, and the
205 receiver outlet temperature is 566 °C. The steam Rankine power cycle has a maximum pressure of

206   115 bar. The cooling method is dry cooling. The TES is achieved by raising MS temperature from 282
207   °C to 566 °C. The TES efficiency is 99%.
208   A scheme of the ISEGS ST facility discussed here after (as well as schemes of PT installations
209   such as the Kramer Junction PT facility) is also provided in [26] and [8]. The reader is referred to
210   these models for the further detailed information eventually needed to complement the information
211   here provided. The power cycle is a relatively simple Rankine cycle of limited efficiency mostly due
212   to the Carnot law.

213

214
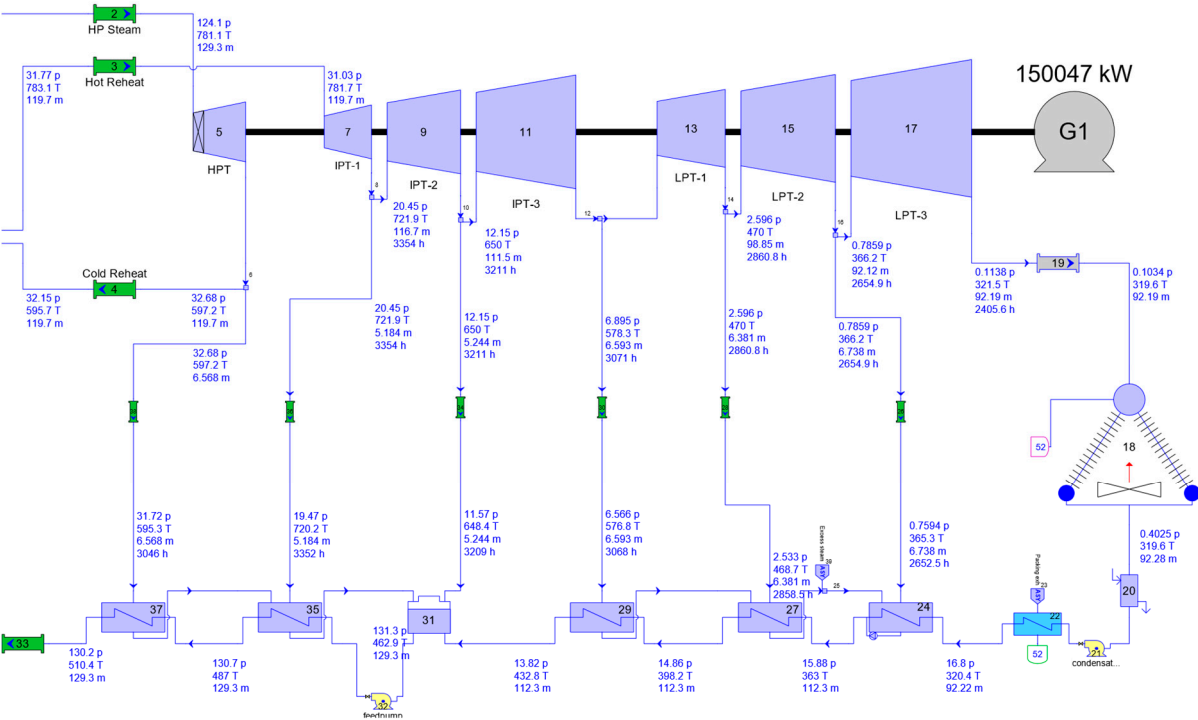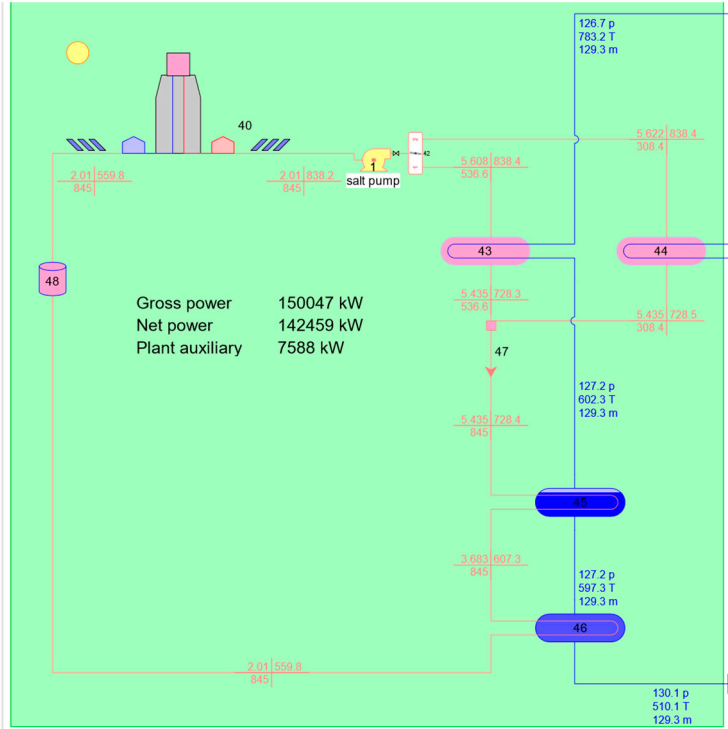
215   **Figure 1.** Thermoflow scheme of the design point balance for the Rice concentrating ST facility.
216   Courtesy of Thermoflow, www.thermoflow.com. All data extracted from public available sources,
217   California Energy Commission.

218   *2.5 Operational parameters*

219   Plant level data of electricity production and NG consumption of CSP plants in the United
220   States are provided in [28]. Data of [28] includes the energy input from both the sun and the NG.
221   Reference design data are provided in [27].
222   Capacity factors of CPS plants with and without NG boost such as ISEGS (Jan-2014 start, ST, no
223   TES), SEGS (various starting dates, Oct-1990 SEGS-IX, PT, no TES) and Solana (Dec-2013 starting
224   date, PT, TES) have been discussed and compared in [8].
225   The capacity factor ε_1 is defined as the ratio of the actual electricity produced in a year E [MWh]
226   with the product of net capacity P [MW] by number of hours in a year:

227    $$\varepsilon_1 = \frac{E}{P \cdot 8760} \qquad (2)$$

228   This capacity factor does not account for the consumption of NG.
229   Ref. [8] suggests as a first option to account for the NG consumption by multiplying the above
230   capacity factor by the ratio of the solar energy input Q_{Sun} to the total solar energy and NG energy
231   input $Q_{Sun} + Q_{NG}$, all in [MWh]:

232    $$\varepsilon_2 = \frac{E}{P \cdot 8760} \cdot \frac{Q_{Sun}}{Q_{Sun} + Q_{NG}} \qquad (3)$$

233   Ref. [8] suggests two other way to evaluate the net capacity factors.
234   A third capacity factor ε_3 is defined as the ratio of the actual electricity produced reduced of the
235   electricity produced by burning the NG in a gas turbine (GT) plant with efficiency η_{GT}=30%, with the
236   product of net capacity by number of hours in a year:

237    $$\varepsilon_3 = \frac{E - Q_{NG} \cdot \eta_{GT}}{P \cdot 8760} \qquad (4)$$

238   A fourth capacity factor ε_4 is finally defined as the ratio of the actual electricity produced
239   reduced of the electricity produced by burning the NG in a CCGT plant with efficiency η_{CCGT}=60%,
240   with the product of net capacity by number of hours in a year:

241    $$\varepsilon_4 = \frac{E - Q_{NG} \cdot \eta_{CCGT}}{P \cdot 8760} \qquad (4)$$

242   An important parameter not accounted for is the requested electricity generation profile.
243   Without TES, the costs per installed capacity are lower, because there is cost associate to the TES and
244   because the turbine is oversized compared to the solar field. However, the electricity production is
245   strongly linked to the sun availability. More than a simple comparison between capacity factors, it is
246   important to compare planned and actual capacity factors to understand the maturity of the
247   technology.

248   *2.6 Prior analyses of operational data*

249   The capacity factors of the three largest CSP projects,
250   –   ISEGS (ST, no TES, NG boost),
251   –   SEGS (PT, no TES, NG boost)
252   –   and Solana (PT, TES, no NG boost),
253   were analyzed in Ref. [8]. Results are summarized below:
254   –   Over the period July 2016 to June 2017 (latest 12 months), without accounting for the NG
255   consumption, ε_1 were 22.98%, 21.59% and 23.67% for ISEGS 1-2-3, 22.54% for SEGS IX and
256   32.65% for Solana.
257   –   By accounting for the consumption of the NG at the actual energy conversion efficiency η of the
258   plant, ε_2 are smaller for ISEGS 1-2-3 at 19.20%, 18.04% and 20.12% and for SEGS IX at 19.91%,
259   while obviously $\varepsilon_2=\varepsilon_1$ for Solana.
260   –   By considering the energy conversion efficiency of a reference GT plant η=30%, the ε_3 are
261   marginally better in ISEGS 1-2-3 and SEGS IX, while $\varepsilon_3=\varepsilon_1$ for Solana.

262   –   Finally, by accounting for the consumption of the NG at the energy conversion efficiency of a
263   reference CCGT plant η=60%, ε_4 are much smaller for ISEGS 1-2-3 at 15.83%, 14.80% and 17.07%,
264   and much smaller for SEGS IX at 17.91%, while $\varepsilon_4 = \varepsilon_1$ for Solana.

265 This analysis confirms the well-established fact [29], [30], [31], [32], [33], [34] that TES plays a
266 significant role in producing much higher capacity factors in present installations, as by TES the
267 power available to the turbine is extended but it is also reduced.

268 *2.7 A critique to the boost by natural gas*

269   The above analysis shows as the use of NG to boost the electricity production in a CSP plant is
270 not motivated, being the fuel energy used at a much lower efficiency than in a CCGT plant, and
271 everything but cost effective. While the hybridization with fossil fuels may be motivated by policies
272 pushing renewable energy production rather than the reduction of fossil fuel usage, the actual
273 benefits in terms of pollution reduction and affordability of energy are quite questionable [8]. Also
274 considering all the issues of integrating intermittent, variable renewable energy electricity into the
275 grid [35], [36], [37], there is no point for a better environment and a better economy of fostering
276 hybridization of CSP with fossil fuel plants as the simple upgrade of traditional plants burning fossil
277 fuels possibly including much cheaper solar ponds costs less while also reducing fossil fuel
278 consumption.
279   CCGT plants can work with an efficiency as high as 62.21% (the 605 MW Bouchain power plant
280 [38], [39]) without any of the constraints of the renewable energy plants. The Bouchain power plant
281 replaces a prior coal plant on 25% of the footprint of the old plant. It is generating more power with
282 50% less CO_2 emission.
283   CCGT plants do not have the constraints of the operation of renewable energy plants such as
284 solar plants. These plants have theoretically the opportunity to operate 24/7 all the year round except
285 than the periods of the scheduled maintenance. Their capacity factors can exceed 90% if contributing
286 to the base-load, or at a lesser extent to match the spikes in the load demand or to supplement the
287 intermittent renewable energy supply. In 2015, the CCGT plants of the US have been operated with
288 average capacity factors of 56% [40].
289   While many policies dedicated to CSP still consider hybridization to make the overall CSP
290 investment more profitable by increasing the usage of the power plant and saving the costs of TES,
291 CSP should not be coupled to the burning of fossil fuels. In our opinion, CSP ST only makes sense as
292 a standalone technology that does not require any fossil fuel.

293 *2.8 Analysis of latest costs and production data*

294   Table 2 provide the latest costs and production data of the most recent CSP ST and PT
295 installations. Opposite to many projections in the literature, costs are here actual, as actual is the
296 production. As there are only 2 CSP ST projects operational worldwide with a significant capacity
297 >50 MW, ISEGS and Crescent Dunes, the first without TES and the second with TES, we also use
298 data of 2 CSP PT projects with and without TES, Solana and SEGS, to make a minimal statistic based
299 on facts.
300   The ISEGS CSP ST plant had a cost (2014 values) of 2,200 m$ for 377 MW of capacity, or 5,9836
301 $/kW. In terms of 2017 values (US inflation calculator [101]) this corresponds to 2,294 m$ and 6,084
302 $/kW. The plant has no TES. The heliostat solar-field has an aperture area of 2,600,00 m², the
303 heat-transfer fluid is water/steam, the receiver inlet temperature is 249 °C, the receiver outlet
304 temperature is 565 °C. The Rankine power cycle max pressure is 160 bar. The latest production data
305 of ISEGS [8], [12], [13], [14], [15] indicates capacity factors of not more than 22-23% despite burning
306 substantial amounts of NG translating in significant additional generating costs and pollution, with
307 the actual capacity factor drastically reducing of more than one third to less than 15% once the
308 consumption of NG is properly accounted for at the fuel energy conversion efficiency of a reference
309 CCGT. The ISEGS power plant was approved in 2014 to burn up to 525 million cubic feet of NG per
310 year [41] and in 2014, the plant emitted 46,084 metric tons of CO_2 by burning NG, that is twice the
311 pollution threshold at which power plants and factories in California are required to participate in

312   the state's cap and trade program [42]. While the planned electricity generation was an optimistic
313   1,079,232 MWh/year [12], or an annual solar-to-electricity efficiency of 28.72%, the actual data [13],
314   [14], [15] for the year 2014, 2015 and 2016 indicate an actual production of 419,085, 653,122 and
315   703,039 MWh/year despite the huge consumption of NG 774,525, 1,245,986 and 1,290,308 MMBtu to
316   boost production. NG consumption of two months of 2014 is missing.

317   The SEGS installation comprises 8 different plants presently operational, built over a time span
318   of several years. It consists of SEGS II located at Daggett, SEGS III–VII located at Kramer Junction
319   and SEGS VIII–IX located at Harper Lake. SEGS I located at Daggett is not operational any more.
320   SEGS X had been in construction but it was never finished. SEGS XI and SEGS XII were planned but
321   never built. The 80 MW SEGS IX has Terminol as receiver fluid, and a temperature at the exit of the
322   483,960 m² solar field of 390 °C. The Rankine power cycle max pressure is 100 bar. As it was claimed
323   in 2002 [43] that based on 1999 cost projections one of the 30 MW SEGS Kramer Junction plants built
324   between 1986 to 1988 required 90 m$ to build, by assuming these costs 1999 values, they correspond
325   to 133.4 m$ of 2017 values (inflation calculator). This translates in an optimistic specific cost of 4,447
326   $/kW. The approximate cost of a project delivering same net capacity of ISEGS ST on SEGS PT
327   technology would be 25% cheaper. However, as these costs for SEGS are based on projections and
328   are not actual costs, and projections are typically non-accurate, these values are not included in
329   Table 2. Production data and NG consumption of the SEGS facility is estimated from the latest SEGS
330   IX plant data, the more recent and best performing. The plant has no TES. The capacity factors of
331   SEGS IX are not far from the values of ISEGS, despite SEGS IX started operation almost 25 years
332   before ISEGS.

333   The cost of Solana (PT, TES) is approximately 2,000 m$, 10% less than the ISEGS ST facility that
334   was completed only two months later, however for 34% less net capacity [8]. The plant has TES.
335   Solana has a specific cost of 8,258 $/kW 2017 values. The production data of Solana is much better
336   than SEGS and ISEGS, with latest capacity factors of about 33%, even if smaller than the planned
337   43.1%. Solana is by far the best performing large CSP plant in the United States. The solar-field
338   aperture area is 2,200,000 m², the heat-transfer fluid is Therminol VP-1 - Xceltherm MK1. The
339   solar-field Inlet Temperature is 293 °C, the solar-field outlet Temperature is 393 °C. 6 hours TES is
340   obtained by using MS with two tanks. The Rankine power cycle max pressure is 100 bar.

341   The 110 MW Crescent Dunes Solar Energy Project [44], [45], the only other project of reasonable
342   size in the world featuring the CSP ST technology and currently operational, had a cost of 975 m$
343   2015 values, corresponding to 1,015 m$ of 2017. This corresponds to 8,864 $/kW 2015 values or 9,227
344   $/kW 2017 values. The heliostat solar-field has an aperture area of 1,197,148 m², the heat-transfer
345   fluid is MS, the receiver inlet temperature is 288 °C, the receiver outlet temperature is 565 °C. The
346   plant has TES and no boost by NG. The TES has 2-tanks, storage capacity 10 hours, TES achieved by
347   raising salt, temperature from 288 to 565 °C. The Rankine power cycle max pressure is 110 bar.

348   The project started operation in November 2015. While the planned electricity generation was
349   500,000 MWh/year (capacity factor 51.89%), the actual electricity produced in 2016 was only 127,308
350   MWh/year. During the year 2016, the plant was operated 10 months January to October. The plant
351   has been so far out of service for about one half of the lifetime, from November 2015 to July 2017.
352   Crescent Dune was indeed shut-down in October 2016 due to a leak in a MS tank and it returned to
353   operation only in July 2017. By using the actual production of 2016, the capacity factor is only 13%.

354   From Table 2 we may conclude that PT may possibly permit lower costs than ST, while TES
355   significantly add to the cost of the plant, but apart from reliability issues, it also improves the
356   electricity production.

357   According to the latest construction cost data for electric generators installed in 2015 by the US
358   Energy Information Administration [46], capacity weighted costs in $/kW were 1,661 $/kW for wind,
359   696 $/kW for NG, 2,921 $/kW for solar photovoltaic. According to the latest (2017) outlook of cost
360   and performance characteristics of new generating technologies by the US Energy Information
361   Administration [47], solar thermal is about 3,908 $/kW, solar photovoltaic 2,169 $/kW, wind 1,576
362   $/kW, wind offshore 4,648 $/kW, conventional combustion turbine is 1,040 $/kW, advanced
363   combustion turbine is 640 $/kW. We may also conclude from Table 2 that the values of [47] are

364 optimistic, i.e. the actual costs differ considerably from the estimates of expert panels. While Table 8
365 - Cost and performance characteristics of new central station electricity generating technologies of
366 [47] reports a base overnight cost in 2016 (2016 $/kW) of 3,908 for solar thermal, ISEGS, Solana and
367 Crescent Dunes have 2017 costs of 6,085, 8,258 and 9,227 $/kW.
368 　　It must be mentioned that the capacity weighted cost is a measure largely in favor of renewable
369 energy plants, typically delivering much smaller capacity factors than fossil fuel plants. The actual
370 costs of CSP per installed capacity of ISEGS, SEGS, Solana and Crescent Dunes are generally high,
371 and much larger than the planned values. Additionally, the actual production of electricity of ISEGS,
372 SEGS, Solana and Crescent Dunes has been much less than the planned values, and by far much
373 smaller than the values potentially achievable in CCGT plants [8]. In the cases of ISEGS and SEGS,
374 the NG consumption has further impacted on the economy and the emissions [8], even if
375 surprisingly this consumption is not properly accounted for. Opposite to SEGS, the costs of ISEGS
376 and Solana, that started production almost simultaneously, are accurate, similarly to Crescent
377 Dunes, that started production only one year later.
378 　　Maintenance or rectification costs are unknown and hence not included in the table.

379 　　　　**Table** 2 – Actual costs and performances of the ISEGS, SEGS, Solana and Crescent Dunes plants.
380 　　　　　　　　　Notes: [1] SEGS IX only. [2] January to October 2016.

Project	ISEGS 1-3	SEGS II-IX	SOLANA	Crescent Dunes
Type	ST	PT	PT	ST
TES	no	no	yes	yes
NG combustion	yes	yes	no	no
year start	Jan-14	Oct-90 [1]	Dec-13	Oct-15
capacity MW	377	340	250	110
planned solar electricity generation MWh/year	1079232	NA	944000	500000
planned solar capacity factor	32.68%	NA	43.11%	51.89%
latest 12 months capacity factor not accounting for the NG consumption	22.75%	22.54% [1]	32.65%	13.21% [2]
latest 12 months capacity factor accounting for the NG consumption η=60%	15.90%	17.91% [1]	32.65%	13.21% [2]
2017 reference cost m$	2294	NA	2065	1015
2017 specific cost $/kW	6085	NA	8258	9227

381

382 　　Data for ISEGS are from [12], [13], [14], [15], data for Solana are from [48], [49], data for Crescent
383 Dunes are from [44], [45], and data for SEGS IX are from [50], [51] as per the retrieved date.

384 **3. Survey of development trends in CSP ST technology**

385 　　In section 2 we provided the actual data of power plants currently operational, including
386 energy outputs and costs of ISEGS (ST), SEGS (PT), Solana (PT, MS TES) and Crescent Dunes (ST,
387 MS TES). ISEGS and Crescent Dunes are the state-of-the-art of the operational CSP ST technology.
388 Based on the real-world experience, the outlook of the CSP ST technology is less brilliant than
389 expected by projections. Hence, there is an urgent need to further progress the technology rather
390 than promoting production of sub-standard plants. Here we survey the developments being sought
391 to improve the current CSP ST technology, with the advertence that the discrepancies in between

actual and projected costs and production data make the claims of the literature speculative. Goal of the survey is only to list the most promising development trends.

On the bright side, as explained in [52], [53], what is called the "*learning rate*", i.e. the cost reduction following the expansion of a technology, may give hope. The short-term survival of CSP depends on accelerated expansion and sufficient cost decrease. Ref. [52] identified the learning rate of CSP and found that it exceeded 20% in the last 5 years. Each time the global CSP capacity doubled, investment costs decreased by over 20%. While this figure may be optimistic, as it is larger than prior estimates such as [102], [103] and [104], and it is still based on a very scattered and incomplete data base, for sure there is a learning rate. Ref. [52] found the learning rate to be highly volatile, reflecting the start-stop pattern of the expansion of CSP experienced so far. Hence, continuity in the R&D effort as well as in the development of an industrial product may ultimately deliver the sought benefits from CSP. Latest cost reductions mentioned in [53] are certainly an indication of the benefits of expanding the CSP ST technology know-how.

Design, construction and operating technical and economic issues are considered in the literature to various extents. CSP ST have many variants for receivers, working fluids, power cycles, type, number and layout of heliostats, height of tower, condenser, turbine, heat exchangers and TES. As an example of a preliminary introductory survey, Ref. [54] examines some of the main parameters of existing plants, solar energy to electricity conversion efficiency, and mirror and land area per MW_e of capacity, packing density, configuration of the field layout, receiver size, tower height and cost of the plant.

3.1 Energy storage and heat transfer fluid

Here we report on the improvement being sought by using a TES with different options for the receiver and the TES fluids. This is the main area of development being considered, as the added value of CSP compared to other renewables is the ability to produce electricity potentially 24/7 through TES.

TES is the key to achieve high capacity factors and avoid NG boost. TES allows improved dispatch-ability (generation on demand) of power from a CSP plant [19]. TES drastically increases the annual capacity factor [8]. The MS TES technology is the best avenue to generate non-intermittent electricity with CSP and achieve capacity factors above 0.3, and potentially up to 0.4. A 10 hour TES eliminates the need for a NG back up or boost of electricity production at sunrise and in the evening peak hours [8].

Next generation CSP plants will very likely consist of four major units, solar field to concentrate the sun light energy, ST MS receiver to convert the solar energy into thermal energy, TES section to store the thermal energy using the MS, and finally power block generating electricity through a steam turbine. While the cost will further increase because of the TES, it will be paid back by the increased production and dispatch-ability.

The current best RF and TES fluid is MS that, however, has the drawback of having low degradation temperature and high melting temperature, in addition to other downfalls such as corrosion and heat tracing. Solar salt, 60% $NaNO_3$ and 40% KNO_3, is used as a low-cost RF and TES fluid. MS temperatures typically go up to 565 °C. This permits superheated steam generation. MS has good heat transfer characteristics [55]. As major downfalls, the salt is freezing below 220 °C, heat tracing is required, and draining of receiver and other system components during the night must be provided. Furthermore, the salt may degrade at temperatures higher than 600 °C and depending on salt quality it can generate corrosion of metallic components [55].

Alternative fluids are therefore under investigation for a broader range of operation and for cost and performance advantages, as RF and / or the TES fluid. The power block fluid is usually water/steam, but other fluids are also considered for the power block, as it is discussed in another paragraph. There is obviously the opportunity to use a single fluid as receiver, TES and power block fluid. Water/steam is the most obvious example.

Ref. [56] reviewed various types of RF including air, water/steam, thermal oils, organic fluids, molten-salts and liquid metals. The different alternatives were compared with reference melting

443   temperature, thermal stability and corrosion with stainless steels and nickel based alloys the piping
444   and container materials. MS shows advantages operating up to 800 °C.

445   Different alternatives for the RF are mentioned in [55]. The presentation includes alternative RF
446   as well as receiver technologies. MS, water/steam, air in open/closed systems, liquid metals, solid
447   particles and other gases are considered as heat transfer medium. Classification is by maturity of
448   technologies. It includes MS and water/steam as state of the art technology, open volumetric air
449   receiver as "first-of-its-kind" technology, then pressurized air receivers as technology in pilot phase,
450   liquid metals and solid particles as technology under development. The different receiver
451   technologies proposed in [55] are reviewed in a subsequent specific paragraph.

452   The impact of the fluid in a flat plate, high temperature, TES unit with flat slabs of phase change
453   materials is studied in [57]. Six gaseous and liquid fluids are compared. For the capacity rate
454   considered, liquid sodium was the best performing (99.4% of the ideal electricity to grid). Solar salt
455   achieved a 93.6% performance. Atmospheric air, air at 10 bars, s-CO_2 at 100 bar and steam at 10 bar
456   achieved performances between 87.9% and 91.3%. The work concludes that gases are comparable to
457   liquids as TES fluids for the specific application and it mentions that gases may also be used as the
458   working fluid in the power block.

459   CSP TES systems are also reviewed in [58]. Various aspects are discussed including trend of
460   development, different technologies of TES systems for high temperature applications (200–1000°C)
461   with a focus on thermochemical heat storage, and storage concepts for their integration in CSP
462   plants. TES systems are considered a necessary option for more than 70% of the new CSP plants
463   being developed. Sensible heat storage technology is the most used TES in CSP plants in operation,
464   for their reliability, low cost, easy to implementation and large experimental feedback. Latent and
465   thermochemical energy storage (TCES) technologies have much higher energy density. This gives
466   them better perspectives for future developments. TCES are specifically covered in a following
467   paragraph. New concepts for TES integration include coupled technology for higher operating
468   temperature and cascade TES of modularized storage units for intelligent temperature control.

469   The current commercial TES systems used in CSP plants either steam accumulators or MS are
470   reviewed in [59]. The economic value of the TES system is assessed by the calculation of the LCOE,
471   an economic performance metric, of the TES itself rather than the full plant. Calculations were done
472   for different plant configurations and storage sizes varying from 1 to 9 h of operation at full capacity.
473   LCOE is shown to be a valid argument for the selection of the TES, even if other aspects not included
474   also play a relevant role.

475   The opportunity to adopt particle suspensions as RF, TES fluid, and power block fluid is
476   considered in [60]. Values of the heat transfer coefficient up to 1,100 $W/m^2/K$ (bare tubes) and 2,200
477    $W/m^2/K$ (finned tubes) were obtained for operation of a pilot plant at low superficial gas velocities of
478   0.04–0.19 m/s limiting heat losses by the exhaust air. Despite additional costs for particle handling
479   and an appropriate boiler, the required overall investment and operating costs are significantly
480   lower than the reference MS system, leading to a reduction in LCOE from approximately 125 €/MWh
481   to below 100 €/MWh.

482   The developments of the last five years and expected for the near future of the most important
483   components of a CSP ST are water/steam, air or CO_2 power cycles; water/steam, MS, liquid metals,
484   particles or chemically reacting fluids and the RF; design of heliostats; design of receivers,
485   volumetric, tubular, solar particle receivers; TES and hybridization are all reviewed in [61]. They
486   conclude that there will certainly be an increased number of CSP ST in the near future, but with a
487   significant hold-back until standardization and experience is gained. Within the next 5 years, plants
488   will use either MS or water/steam as the receiver fluid, but most of them will have MS TES. In a 10
489   years' time, more plants will be MS with TES. However, according to [61], "The commercial plant
490   designs in 10 years will look not much different than the commercial plant designs today", which is
491   a not desirable option.

492   Thermochemical energy storage has been proposed to replace the TES. This opportunity is in a
493   very early stage of development. In addition to the classic TES design with two tanks of a properly

494 selected TES fluid, TCES systems have been also proposed. TCES is the reversible conversion of
495 solar-thermal energy to chemical energy.
496   The TCES systems are reviewed in [62]. TCES has high energy density and low heat loss over
497 long periods than the MS TES. CSP plants with TCES systems are modelled, and sample
498 computational results are provided for ammonia and methane systems with two gas storage
499 options. The gas storage is identified as the main cost driver. The compressor electricity
500 consumption is identified as the main energy driver.
501   Ref. [63] reports of a pilot-scale redox-based TCES system. The storage unit is made of inert
502 honeycomb supports (cordierite) coated with 88 kg of redox active material (cobalt oxide). When
503 crossing respectively the reduction/oxidation temperature of the Co_3O_4/CoO pair, the heat absorbed
504 or released by the chemical reaction allows to store or release energy at constant temperature. Within
505 the limit of a campaign of 22 thermochemical charge/discharge cycles, there was no measurable
506 cycle-to-cycle degradation. The system average capacity was very close to the ideal case. The TCES
507 system offers a storage capacity of 47.0 kWh vs. the 25.3 kWh of the same volume of a sensible-only
508 storage unit made of uncoated cordierite honeycombs.

509 *3.2 Power cycles and power cycles fluids*

510   Here we report on the improvement being sought by using different power cycles and power
511 cycle fluids. This is an area of development receiving significant attention that may possibly produce
512 results within the next decade.
513   Supercritical steam [64] and supercritical CO_2 (sCO_2) [65] power cycles are being considered to
514 improve the conversion efficiency thermal-electric cycles. Ref. [66] computed the thermodynamic
515 irreversibility such as convective and radiative loss on tower receiver and thermal resistance in heat
516 exchangers. Increasing the receiver working temperature increases both thermal and exergy
517 conversion efficiencies only until an optimum temperature is reached. The optimum temperature
518 increases with the concentration ratio. Increasing the concentration ratio, the conversion efficiency
519 increases only until an optimum concentration ratio is reached. Increasing the end reversible engine
520 efficiency increases the thermal conversion efficiency until a maximum value is reached. Then, the
521 conversion efficiency drops dramatically.
522   The performance of an integrally geared compressor-expander recuperated recompression
523 cycle with sCO_2 as the working fluid is modeled in Ref. [67]. Mostly through reduced power block
524 cost and a better cycle model, the LCOE is computed to be 5.98 ¢/kWh.
525   Advanced power cycles under consideration for CSP are reviewed in [68]. Supercritical steam
526 turbines are attractive at large scale but presently commercial products are too large for today's CSP
527 ST plants. SCO_2 closed loop Brayton cycles are early in their development but promise high
528 efficiency at reasonable temperatures across a range of capacities. In perspective, these cycles may
529 significantly lower the costs. GT combined cycles driven by CSP are one of the highest efficiency
530 options available. Other bottoming and topping cycle configurations are also considered. High
531 temperature component demonstration is indicated as a critical factor.
532   Three different sCO_2 power cycles applied to a high temperature ST CSP system are considered
533 in Ref. [69]. Maximum temperatures are up to 800 °C. The fluid transferring energy from the receiver
534 to the power block is $KCl-MgCl_2$ MS. The highest efficiency at design conditions is achieved by the
535 Recompression with Main Compression Intercooling (RMCI) configuration with a solar energy to
536 electricity efficiency of 24.5% and a maximum temperature of 750 °C. The capacity factor is 18.4%.
537 The performance decay from design to average yearly conditions is mostly due to the optical and
538 thermal efficiencies reduction respectively of -10.8% and -16.4%.
539   Several current sCO_2 Brayton cycles for integration into a MS CSP ST system are reviewed in
540 [70]. The intercooling cycle can generally offer the highest efficiency, followed by the partial cooling
541 cycle, and the recompression cycle. The pre-compression cycle can yield higher efficiency than the
542 recompression cycle when the compressor inlet temperature is high. The increase in the hot salt
543 temperature cannot always result in an efficiency improvement. The partial cooling cycle can offer
544 the largest specific work, while the recompression cycle and the split expansion cycle yield the

545   lowest specific work. The MS temperature differences with the simple recuperation cycle, the
546   partial-cooling cycle, and the pre-compression cycle are slightly larger than those with the
547   recompression cycle, the split expansion cycle, and the intercooling cycle. Reheating can decrease the
548   system efficiency in the cases with high hot MS temperature. Larger MS temperature difference may
549   be achieved without reheating than with reheating. While current sCO_2 Brayton cycle offer high
550   efficiency, challenges for integrating them includes the specific work that is relatively small, and the
551   temperature difference across the solar receiver that is narrow.
552   More efficient Rankine power cycles are studied in [71]. The temperature and pressure of the
553   main steam and the reheating pressure affect the temperature of the MS in the receiver. If the
554   temperature increases, the receiver efficiency decreases but the power block efficiency increases. If
555   the pressure at the inlet of the turbine increases, the efficiency of the power block increases even
556   more than by increasing the temperature. The reheating pressure is the most influential factor on the
557   plant efficiency. A high reheating pressure decreases the plant efficiency. The best efficiencies were
558   obtained for the supercritical cycle with a low reheating pressure and high temperature. The
559   subcritical cycle at high pressure and temperature performed closely. The investment cost of the
560   different cycles increases with the pressure and the temperature of the power block. Subcritical
561   cycles are less expensive than supercritical cycles even if the cost increase is balanced by the
562   efficiency increase. Subcritical cycles working at 16 MPa and supercritical cycles working with low
563   reheating pressure deliver the same cost per MW_e.
564   Energy and exergy analyses of sCO_2 recompression Brayton cycles are proposed in Ref. [72].
565   The heliostat field layout is optimized for the optical performance on an annual basis. A
566   recompression Brayton cycle uses the heat collected at the receiver. An auxiliary boiler is added
567   prior to the turbine to keep the turbine inlet temperature constant. The net power output is constant
568   40 MW. The highest exergy destruction occurs in the heliostat field. The second highest exergy
569   destruction happens in the boiler's combustion chamber. The combustion exergy destruction rate
570   increases during the winter months when the solar radiation decreases.
571   The thermal performance of an array of pressurized air solar receiver modules integrated to a
572   GT power cycle for a simple Brayton cycle, a recuperated Brayton cycle, and a combined
573   Brayton-Rankine cycle are studied in [73]. The solar receiver's solar energy to heat efficiency
574   decreases at higher temperatures and pressures. The opposite is true for the power cycle's heat to
575   work efficiency. The optimal operating conditions are achieved with a preheat stage for a solar
576   receiver outlet air temperature of 1300 °C and an air cycle pressure ratio of 9, yielding a peak solar
577   energy to electricity efficiency of 39.3% for the combined cycle.
578   Alternative cycles' technology certainly needs more work before introduction in full scale CSP
579   ST plants where water/steam Rankine cycles are the best short-term (10 years' time window)
580   solution. According to [61], citing a private communication, only in perhaps 10 years from now,
581   there could be a shift to supercritical CO_2-based plants.

582   *3.3 Design of solar field and receiver*

583   Here we report on the improvement being sought by redesigning solar field and receiver. This
584   is an area of development also receiving significant attention, that may possibly produce significant
585   results within the next decade.
586   According to Ref. [54], the annual solar energy to electricity conversion efficiency corresponds
587   to an average of about 16%. The packing density has an average of about 20%.
588   A classification by maturity of receiver technologies is proposed in [55] and has been included
589   in a prior paragraph. In addition to MS and water/steam state of the art technologies, open
590   volumetric air receiver, pressurized air receivers, liquid metals and solid particles are all
591   technologies being developed at different stages of evolution. As the receiver design is not
592   decoupled from the design of the solar field, here we couple together these two aspects.
593   Gas receivers, liquid receivers, and solid particle receivers are reviewed in [74]. Higher
594   thermal-to-electric efficiencies of 50% and higher may be achieved by using sCO_2 closed-loop
595   Brayton cycles and direct heating of the CO_2 in tubular receiver designs, external or cavity, for high

596   fluid pressures of about 20 MPa and temperatures of about 700 °C. Indirect heating of other
597   fluids/materials that can be stored at high temperatures such as advanced MS, liquid metals, or solid
598   particles are also possible, but with additional challenges such as stability, heat loss, and the need for
599   high-temperature heat exchangers.

600   As per [55], strategies aimed at improving MS systems include higher temperature MS, higher
601   steam parameters, smaller heat exchanger, smaller storage, less critical receiver temperature
602   operation. Means to improve the receiver efficiency include reduction of thermal losses, cavity
603   arrangement, face down can design, standard vacuum absorber for first temperature step, and
604   selective coatings for higher absorption of solar radiation [55]. Optimization of operation includes
605   real time aim point strategy for homogenous receiver temperature, solar pre-heating of receiver,
606   faster start-up and elimination of draining of receiver during clouds [55].

607   The improvement of the solar flux intercepted by the receiver to increase the peak flux is
608   considered in [75]. They propose a new receiver, named Variable Velocity Receiver (VVR), Figure 2,
609   consisting of a Traditional External Tubular Receiver (TETR) equipped with valves permitting the
610   division of each panel in two independent panels. This increases the velocity of the heat transfer
611   fluid in specific zones of the receiver avoiding tube overheating. The novel design also permits
612   better aiming strategies, for an improved optical efficiency of the solar field and a possible reduction
613   of the number of heliostats.

614
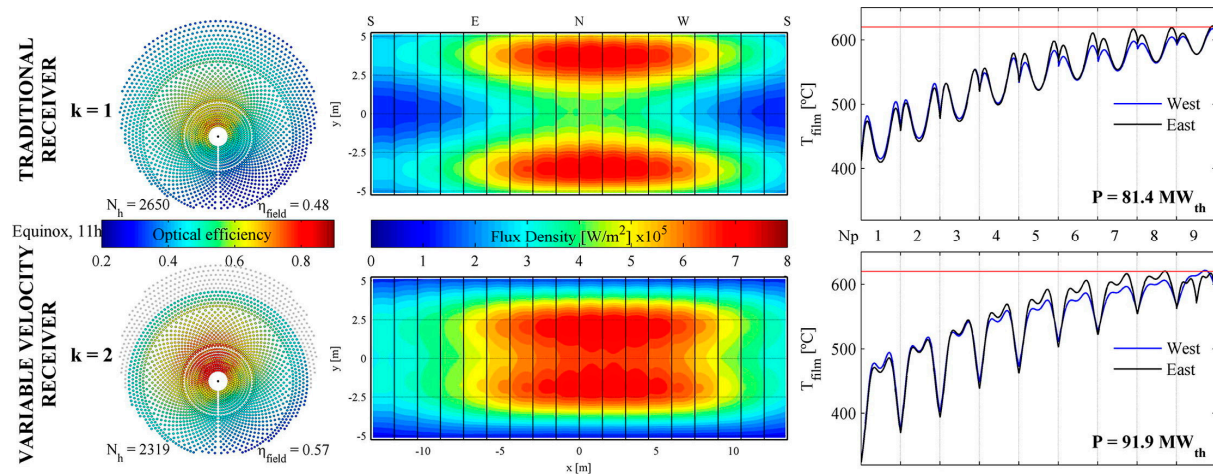
615   Figure 2 – Operation of the novel Variable Velocity Receiver proposed in [75] vs. a Traditional
616   External Tubular Receiver. Reprinted from Applied Thermal Engineering, Vol. 128, M.R.
617   Rodríguez-Sánchez, A. Sánchez-González, D. Santana, Feasibility study of a new concept of solar
618   external receiver: Variable velocity receiver, Pages No. 335-344, Copyright (2018), with permission
619   from Elsevier.

620   The size of the solar field required by a VVR is 12.5% smaller than the size required by a
621   traditional TETR. Additionally, the VVR provides advantages for the winter operation when the
622   panels can be split in two, increasing the number of passes and the velocity of the heat transfer fluid.

623   High temperatures, thermal shocks and temperature gradient from a high, non-homogeneous
624   and variable flux on the receiver walls are responsible for significant stresses. These stresses reduce
625   the life-span of the receiver. Ref. [76] proposes an open loop approach to control the flux density
626   distribution delivered on a CSP ST flat plate receiver. Various distributions of aiming points on the
627   aperture of the receiver are considered. The approach provides interesting indications for the control
628   of the heliostats that may drastically improve the life-span of the component.

629   The optimization of a solar field layout with heliostats of different size is considered in [77].
630   Although the use of a single heliostat size is openly questioned in the literature, there are no tools to
631   design fields with heliostats of different sizes in the market. The paper addresses the problem of
632   optimizing the heliostat field layout with two heliostats' sizes.

633   Ref. [78] numerically studied the influence of wind and return air on a volumetric receiver.
634   Figure 3 presents a sketch of the receiver. The volumetric receiver is a highly porous material which

635 absorbs solar radiation at different depth through its thickness. The effective area for solar
636 absorption is larger than that of thermal radiation losses. A fan draws air through the absorbent
637 pores, and the convective flow captures the heat absorbed. Thanks to the volumetric effect [79], the
638 absorber thermal radiation loss is reduced.
639   Ref. [80] optically simulated the solar light radiation transmission from the heliostat field to a
640 pressurized volumetric receiver. The optical efficiency of the heliostats' field and the local heat flux
641 distribution within the absorber is computed as a function of time and date, heliostats tracking error
642 and receiver mounting height. The heat flux distribution within the absorber is non-uniform. The
643 maximum heat flux density at the top area is up to $2.58 \cdot 10^9$ W/m^3. The pattern of field efficiency and
644 maximum heat flux density of the absorber resembles those of the solar altitude angle during a
645 day/year. The annual mean field efficiency and the maximum heat flux of the absorber decrease as
646 the tracking error increases. As the receiver mounting height increases, both these parameters are
647 marginally increasing.

648
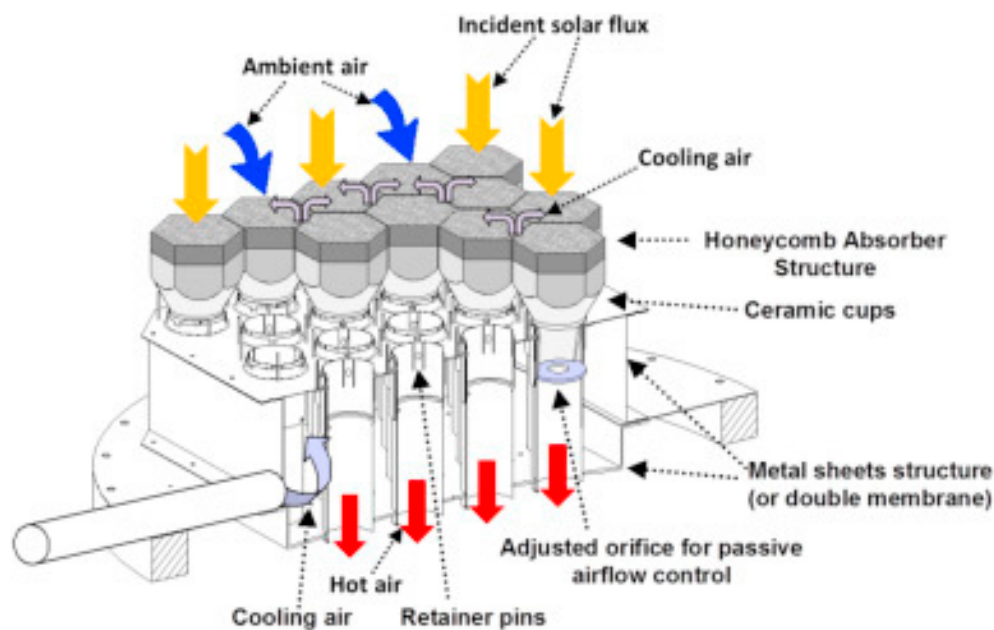
649 **F**igure 3 – Volumetric receiver used in [78]. Reprinted from Energy, Vol. 94, Roldán, M.I.,
650   Fernández-Reche, J. and Ballestrín, J., Computational fluid dynamics evaluation of the operating
651   conditions for a volumetric receiver installed in a solar tower, Pages No. 844-856, Copyright (2016),
652   with permission from Elsevier.

653   A dual-receiver with a surrounding solar field is proposed in [81]. The design couples an
654 external boiling receiver and a cavity superheating receiver. The design provides a simple yet
655 controllable heat flux distribution on both sections. The dual-receiver may produce superheated
656 steam of 515 °C and 10.7 MPa with a solar heat absorbing efficiency of 86.55%. The efficiency
657 improvement compared to two-external cylindrical receivers is 3.2%.
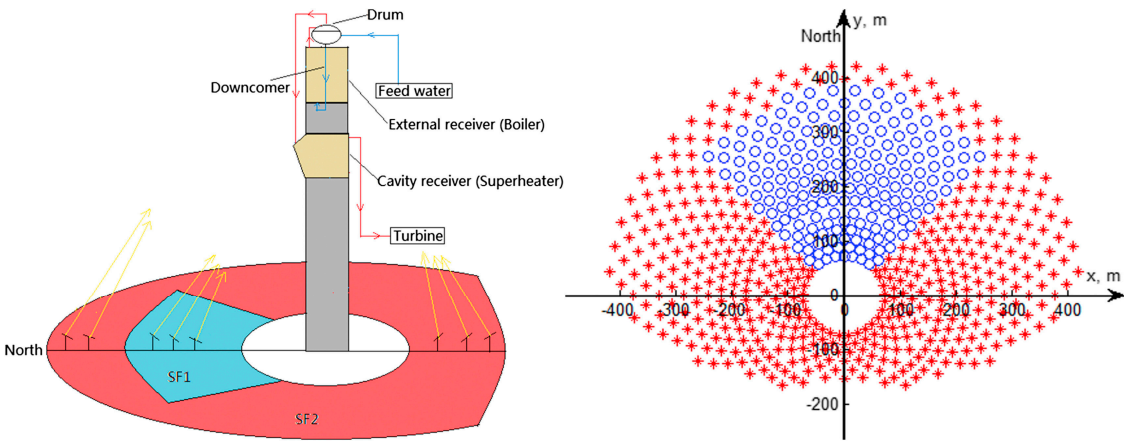
Figure 4. Schematic diagram of the tower and heliostat field for the dual-receiver proposed in [81]. Reprinted from Applied Thermal Engineering, Vol. 91, Luo, Y., Du, X. and Wen, D., Novel design of central dual-receiver for solar power tower, Pages No. 1071-1081, Copyright (2015), with permission from Elsevier.

A Multi-Tube Cavity Receiver (MTCR) was optically modelled in [82]. The solar flux exhibits a significant non-uniformity, showing a maximum flux of $5.1 \cdot 10^5$ W/m² on the tubes. When considering the random effect on the solar flux distribution, it is a good practice to treat the tracking errors as the random errors of the tracking angles. Multi-point aiming strategy of tracking helps to homogenize the flux and reduce the energy mal-distribution among the tubes. The tubes absorb 65.9% of the energy. The optical loss can be reduced significantly by the cavity effect, especially when the coating absorptivity is relatively low.

Heliostats account for about 50% of the capital cost of CSP ST plants. In conventional heliostats with vertical pedestals and azimuth-elevation drives, the support structure contributes 40–50% of this cost due to heavy cantilever arms required by the large spanning structures. Additional costs are imposed by expensive, difficult to maintain, drive mechanisms. Ref. [83] shows that a tripod heliostat substantially addresses these shortcomings for heliostats with aperture areas of 62 to 100 m². Ray-tracing simulations are included to estimate the performance penalties due to deformation under gravity and wind loads. The additional energy collection by a less-stiff, larger heliostat more than offsets the waste due to the greater deformation. The economics of CSP ST plants are strongly dependent on the cost of the heliostats rather than their optical performance. The cost of a tripod heliostat is reduced to $72/m² which is less than half that of the conventional systems.

The thermal performance of a cavity receiver in a CSP ST plant that relies on the spatial relationship of its polyhedral geometric inner surfaces is studied in [84]. Based on model results, the thermal efficiency of the cavity receiver is shown to increase with the increase of incident heat flux. When the width-depth ratio decreased, the cavity efficiency increased first and then decreased. The total heat loss of the receiver varied differently with the increase of the heat absorption area to the aperture area ratio.

The thermal efficiency of multi-cavity CSP ST receivers was modelled in [85]. There is an optimal aperture flux that maximizes the local efficiency. This optimum is constrained by the maximum receiver working temperature. For this aperture flux, the thermal efficiency, receiver temperature, and RF temperature are calculated for an optimized flux distribution. In the proposed case study, it was found that a RF with a minimum convection coefficient between 250 and 500 W/m²/K, permits to achieve a receiver thermal efficiency greater than 90%.

An array of high temperature pressurized air based solar receivers for Brayton, recuperated, and combined Brayton-Rankine cycles was investigated in [86]. The cluster of 500 solar receiver modules, attached to a hexagon-shaped secondary concentrator and arranged side-by-side in a honeycomb-type structure following a spherical fly-eye optical configuration, yield a peak solar energy to electricity efficiency of 37%.

697   Ref. [87] studied beam-down concentrating solar tower (BCST). BCST are known for easy
698   installation and maintenance as well as lower convection heat loss of the central receiver. A
699   point-line-coupling-focus BCST system using linear Fresnel heliostat as the first stage concentrator
700   (heliostat) and hyperboloid/ellipsoid reflector as the tower reflector is proposed. Theoretical
701   investigation on the ray concentrating mechanism with two commonly used reflector structures,
702   namely, hyperboloid and ellipsoid, indicate that the ellipsoid system is superior in terms of
703   interception efficiency over the hyperboloid system due to smaller astigmatism at the central
704   receiver aperture, especially at larger facet tracking error [87]. The ellipsoid reflector shows
705   significantly lower tower reflector shading efficiency. This is the result of the larger tower reflector
706   surface area compared to that of the hyperboloid reflector. The total optical efficiency of the
707   hyperboloid system is always better than that of the ellipsoid system. This efficiency gap decreases
708   as the ratio increases. The hyperboloid tower reflector is claimed to be more promising and practical
709   for the system investigated.

710   Volumetric air receivers were studied in [88]. This component consists of a high temperature
711   resistant cellular material which absorbs radiation and transfers the heat to an air flow which is fed
712   from the ambient and from recirculated air. It is called volumetric, because the radiation may
713   penetrate the "volume" of the receiver through the open, permeable cells of the material. In this way,
714   a larger amount of heat transfer surface supports the solid to gaseous heat transfer in comparison to
715   a tubular closed receiver. The heated air is directed to the steam generator of a conventional steam
716   turbine system. Ref. [88] uses an advanced cellular metal honeycomb structure. It consists of winded
717   pairs of flat and corrugated metal foils. Several variations of the pure linear honeycomb structure
718   have been introduced to increase local turbulence and radial flow.

719   While some of these technologies may be easily implemented in future installations, those more
720   sophisticated and innovative certainly require further studies.

3.4 Manufacturing and materials

722   New materials and manufacturing processes are urgently needed to reduce costs and improve
723   reliability and life-span of current designs. New materials are also needed for operation of
724   components with higher temperatures and with reduced heat losses to also improve efficiency.

725   While there is an abundant literature about new design of cycles, solar fields and receivers, TES
726   system, and receiver and power block fluids, manufacturing processes and new materials are only
727   marginally covered in the literature despite their huge impacts on costs and production of the CSP
728   ST plants. Manufacturing of solar plant components is almost ignored.

729   Materials studies are mostly focused on the coating of the receiver. Solar receivers are presently
730   mostly coated with a high sunlight absorptivity layer applied over the bare surface of the absorber
731   receiver's tubes. Pyromark 2500 is the present standard coating. The coating enhances absorptivity
732   and light-to-heat conversion. Ref. [89] studied the effect of the optical properties absorptivity and
733   emissivity of these coatings on the thermal performance of a MS external receiver. Solar selective
734   and non-selective coatings were analyzed and compared against the standard coating. The thermal
735   efficiency increases up to 4% with the absorptivity of the coating. The emissivity has a very minor
736   effect on the thermal performance of the receiver at its nominal working temperature. The efficiency
737   only increases 0.6% when the emissivity of the coating decreases from 0.9 to 0.5. Improving the
738   absorptivity of a non-selective coating leads to higher thermal efficiency than using a selective
739   coating for current MS temperatures. For superheated steam cavity receivers, the effect of using a
740   selective coating is noticeable at temperatures greater than 500 °C.

741   Ref. [90] also studied solar absorber coatings. The LCOE metric is used to attribute value to any
742   high-temperature absorber coating. The LCOE gain efficiency is demonstrated on three different
743   solar absorber coatings: Pyromark 2500, lanthanum strontium manganite oxide (LSM), and cobalt
744   oxide (Co_3O_4). These coatings were used in a 100 MWe central tower receiver. Depending on the
745   coating properties, an optimal reapplication interval was found that maximizes the LCOE gain
746   efficiency. Pyromark 2500 paint enables a higher LCOE gain efficiency (0.182) than both LSM (0.139)
747   and Co_3O_4 (0.083). The solar absorptance is by far the most influential parameter. The

748 cost-effectiveness of Pyromark can be outperformed by a coating that would have a high initial solar
749 absorptance (>0.95), a low initial degradation rate (<$2 \cdot 10^{-6}$ cycle^{-1}), and a low cost (<$500k per
750 application).
751   A novel MoSi2–Si3N4 hybrid composite, Figure 5 was studied in [91]. The MoSi2–Si3N4
752 absorber deposited onto Inconel substrate and capped with a Si3N4/Al2O3 layer on top is a
753 promising selective coating for receivers operating in air at temperatures about 600 °C. Stacks with
754 the Inconel/MoSi2-Si3N4/Si3N4/ Al2O3 structure on Inconel substrate show indeed good thermal
755 stability in air.

756
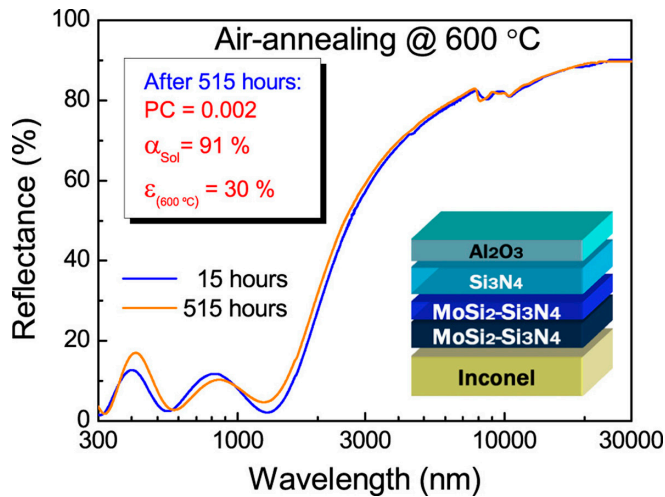
757 **F**igure 5. Reflectance of new coating from Ref. [91]. Reprinted from Solar Energy Materials and Solar
758   Cells, Vol. 174, Rodríguez-Palomo, A., Céspedes, E., Hernández-Pinilla, D. and Prieto, C.,
759   High-temperature air-stable solar selective coating based on MoSi 2–Si 3 N 4 composite, Pages No.
760   50-55, Copyright (2018), with permission from Elsevier.

761 *3.5 Integrated solar combined cycle systems*

762   Here we report on the integration of CSP ST with CCGT or other plants, such as desalination
763 plants.
764   Despite current policies may favor the opportunity of integrating CSP ST with CCGT, as
765 explained in a prior section we do not believe CSP ST should be coupled to the burning of fossil
766 fuels. While the use of NG in a boiler that supplement the solar field in the production of steam is
767 common practice but it is not the best one as NG could be better used at double the thermal
768 efficiency in a CCGT plant, it is more interesting opportunity to consider even if still questionable
769 the coupling of a CSP ST plant with a CCGT plant.
770   Integrated solar combined cycle systems (ISCCS) are reviewed in Ref. [92]. ISCCS consist of
771 three major components, CCGT, ST steam generator and solar field. The study indicates that very
772 limited research has been directed so far toward the development of ISCCS with ST. Most of the
773 ISCCS plants in operation today employ the PT technology. No known commercial ST ISCCS plant
774 is operational in 2015. The study of ISCCS with ST is therefore an area of potential improvements
775 still unexplored.
776   CSP PT and CSP ST coupled to a CCGT were modelled in [93]. The solar Rankine cycle is a
777 single reheat regenerative Rankine cycle. The CCGT plant features a commercial gas turbine, with a
778 dual pressure heat recovery steam generator. MS is the fluid to transfer heat to the water/steam of
779 the solar Rankine cycle. Synthetic oil is used in the CCGT plant. The CSP ST has a higher collection
780 efficiency than the CSP PT. The combined cycle is more efficient than the solar Rankine cycle. The
781 CCGT plant coupled with a CSP ST is found to deliver the highest annual solar-to-electric efficiency
782 of 21.8%.

783   As the integration of renewables with conventional power sources is presently discouraged, it is
784 not expected that power plant burning fossil fuels will be integrated with solar fields, even if this is
785 by far the best opportunity to convert solar thermal energy in electricity.

786   While integration of CSP ST with CCGT does not make too much sense, there is certainly the
787 scope of integrating CSP ST with Multi-effect desalination (MED) to produce electricity and clean
788 water in remote areas. As power and water supply are the two major issues humanity will face
789 during this century, a robust growth of CSP around the world may be integrated with desalination
790 for the next renewable energy breakthrough [94].

791   In desalination, seawater is separated into a low concentration of salts freshwater stream and a
792 high concentration of salts brine. The most relevant desalination technologies are thermal
793 desalination and membrane desalination. Thermal desalination utilizes heat, often by steam, to
794 change phase of the seawater from liquid to vapor. Membrane desalination utilizes pressure, and
795 hence electricity driven pumps, to force water through a semi-permeable membrane. In general,
796 membrane desalination has advantages in terms of energy requirements and it is preferred where
797 salinity is not very high. Seawater reverse osmosis (SWRO) membrane processes require less energy
798 than multi-effect distillation (MED) thermal processes. However, Ref. [95] suggests that, for several
799 locations, for example the Arabian Gulf, CSP plus MED may require 4% to 11% less input energy
800 than CSP plus SWRO. This introduces an interesting opportunity for selected locations where MED
801 may be competitive with SWRO. While SWRO does not need any integration of the desalination
802 plant with the CSP plant, as the electricity needed can be produced everywhere, MED may be easily
803 and conveniently integrated with a CSP saving the condenser costs.

804   MED produces high quality water from sea or brackish water. Concentration of total dissolved
805 solids (TDS) is 25 mg/l or less. MED units range from about 100 m³/day up to 36,400 m³/day. While
806 single units may be utilized in smaller volume applications, multiple units may be combined to
807 further increase capacity [94].

808   In desert installations, far from the coast, the condenser is air cooled, and this limits the
809 expansion of steam in turbine. While in coastal locations the condenser may certainly be, water
810 cooled for better performances of the plant, alternatively, the condenser may also be replaced by a
811 MED thermal desalination module. The steam generated is superheated to 380 °C to 580 °C and the
812 steam temperature for the MED is not higher than 135 °C [94]. Hence, the steam has sufficient energy
813 to produce electricity before entering the MED. If power is the main product, a water condenser may
814 work better. However, where water is more precious than power, and MED is competitive with
815 SWRO, integration of CSP ST with MED is a local renewable energy break-through.

816   Ref. [96] proposed solar thermal sea water desalination, however adopting multi-stage flash
817 evaporation (MSF) rather than MED. The theoretical study considers a ST with a volumetric solar
818 receiver, a power cycle water/steam Rankine, MS as the receiver fluid, MS TES plus the MSF. The
819 seawater is heated by the saturated steam-water mixture coming from the steam turbine. This
820 eliminates the condenser. Considering the advantages MED has vs. MSF [94], presently the primary
821 thermal desalination option, the advantages mentioned in [96] will be further strengthen when using
822 MED.

3.6 Regionalization

824   As a final area of concern, here we report on the improvement being sought in CSP ST
825 technology by specializing the design for a specific geographical location. Places with lot of sun to
826 make plausible CSP ST plant may have very different climate conditions. Proximity to coast,
827 availability of land, orography of land, coupling to desalination, availability of NG, prevailing
828 weather conditions, sand storms, wind load, rainfall, all play a key role to reshape one single design
829 to match local conditions. Despite some design concepts may certainly be shared between many
830 different CSP installations, regionalization plays a significant role in providing the sought outcomes
831 in terms of performance, cost and life span of a plant.

832   The technical, financial and policy drivers and barriers for adopting CSP ST technologies in
833 India were studied in [54]. Especially CSP ST with external cylindrical or cavity receivers with

834   storage look promising. This technology is particularly relevant to the Jawaharlal Nehru National
835   Solar Mission (JNNSM) aimed at achieving grid-connected solar power of 1800 MW by 2022.

836   Ref. [97] reviews the CSP plants installed in India and discusses the growth of the electricity
837   generated by CSP in India, with targets grown to 100,000 MW by 2022.

838   The design and construction of a CSP ST demonstration plant in Saudi Arabia, an area of
839   extreme solar intensity and temperatures, was reported in [98]. The solar receiver was made of alloy
840   steel. Ten heliostats were chosen, featuring two motors were used to control the heliostat rotational
841   and elevation movements. The thermal fluid was a MS mixture 60% $NaNO_3$ and 40% KNO_3. Cold
842   and hot storage tanks were manufactured from steel insulated with calcium silicate from all sides. A
843   one-meter high and one and a half-meter diameter cylindrical vessel was adopted for each of the
844   cold and hot tanks. The design thermal power was 13 kW. The thermal power released by the MS
845   was 12.31 kW. The thermal power transferred to the water/steam was 11.26 kW. The work proves
846   the value of small demonstration plants. Small demonstration plant is needed for regionalization in
847   every location where conditions may differ considerably from the areas of well-established designs
848   to perform a proper regionalization of the design.

849   The energy and exergy analyses of sCO_2 recompression Brayton cycles of Ref. [72] is performed
850   for different locations in Saudi Arabia. The exercise returns a ranking by location based on the
851   selected CSP ST configuration.

852   Ref. [99] simulated the behavior of the Spanish GEMASOLAR plant under different climates.
853   The analysis is performed for different locations of mainland China. An estimation of both annual
854   energy production and return of the investment was provided. Simulations were made with and
855   without hybridization with combustion of fossil fuels and with same or modified nominal power.
856   Annual overall efficiencies were about 14% for the 20 MW power plant (GEMASOLAR nominal
857   power). Down-scaled plants were able of maintaining an efficiency of 14.97% for a 10 MW power
858   plant.

859   Ref. [100] compares under the Algerian climate a Rankine cycle with a tubular water/steam
860   receiver and a Brayton cycle with volumetric air receiver. The tubular receiver Rankine cycle is
861   economically slightly disadvantaged vs. the volumetric air receiver Brayton cycle, but it works better
862   especially under lower solar radiation intensity. The GT requires higher operating temperatures
863   which are usually difficult to reach throughout the year.

4. Conclusions

865   Our analysis builds on actual data of costs and operation of CSP ST facilities.

866   There are only two CSP ST plants of capacity more than 100 MW operational in the world. The
867   largest one, the 377 MW capacity ISEGS, with no TES, has not produced more than 703,039
868   MWh/year in the 3rd year of life (2016), up from the 419,085 MWh/year of the 1st year of life (2014),
869   despite the combustion of huge amounts of NG, still 1,290,308 MMBtu in the 3rd year of life (2016).
870   The planned electricity generation was 1,079,232 MWh/year since 2014. Actual construction cost has
871   been 6,085 $/kW (2017 values). The other plant, the 110 MW Crescent Dunes facility, with TES, has
872   produced in 2016 only 127,308 MWh/year vs. the planned 500,000 MWh/year. Actual construction
873   cost has been 9,227 $/kW (2017 values).

874   The electricity production and the reliability of the plant have been so far worse than the
875   expected. Additionally, the costs have been much larger than what was planned. The real-world
876   experience thus casts considerable doubts on the number being proposed for the CSP ST technology
877   by expert panels and the literature. The CSP ST plant technology is still very far from the standards
878   of conventional power plants in the power industry, where the actual costs and performances are
879   usually close to the planned values. More experience must be gathered to proper develop a
880   technology that appears to be still in its infancy.

881   Having said that, there are certainly many development trends being sought that even if not
882   game changers can make the CSP ST technology much more competitive at least vs. other
883   renewables, wind or solar photovoltaics. As actual numbers are very far from plans, we analyze all
884   these technology updates being sought with the due skepticism. The current trends in the

885 development of CSP ST installations have been reviewed. Improvements are being sought for
886 efficiency of plant, installation cost, life-span and operation cost. Materials and manufacturing
887 processes, design of solar field and receiver, including fluids, cycle and materials, optimal
888 management of daily and seasonal operation of the plant, new TES concepts, integration of solar
889 plant with thermal desalination, integration of solar plant with CCGT installations and finally,
890 specialization and regionalization of the project specification, are the key areas of progress of CSP ST
891 technology.
892   While it is expected that CSP ST installations will grow considerably in the next few years, there
893 is not yet a better solution all-inclusive than the use of MS as RF and TES fluid, with classic solar
894 field heliostats and receivers, driving a water/steam superheated Rankine cycle steam cycle.
895 Manufacturing is a major keyword to cover. The different alternatives that are presently under study
896 at different stages of development may only progress slowly, benefiting from real world experiences
897 requiring time rather than simulations or laboratory experiments. Cost of plants are not expected to
898 reduce drastically, even if convergence on few selected designs of heliostats and receivers could be
899 beneficial to their improvement and cost reduction, with manufacturing of components in large
900 scale and significant feed-backs from real world operation expected to be a major driver of the
901 developments.

902 **Acknowledgments:** The authors received no funding.

903 **Conflicts of Interest:** The authors declare no conflict of interest.

904 **Authors' contributions:** The authors equally contributed to the review of the papers and the writing of the
905 manuscript.

906 **Symbols**
907 η   efficiency
908 ε capacity factor
909 E   electric energy
910 P   electric power
911 Q   thermal energy
912 sCO_2 supercritical carbon dioxide

913 **Acronyms**
914 BCST   beam-down concentrating solar tower
915 CSP   concentrated solar power
916 CCGT   combined cycle gas turbine
917 GT   gas turbine
918 ISCCS   Integrated solar combined cycle system
919 ISEGS   Ivanpah Solar Electric Generating System
920 LCOE   Levelized Cost of Electricity
921 MED   multi effect distillation
922 MS   molten salt
923 MTCR   Multi Tube Cavity Receiver
924 NG   natural gas
925 PT   Parabolic Trough
926 PV   photovoltaic
927 RF   receiver fluid
928 RMCI   Recompression with Main Compression Intercooling

929   SEGS   Solar Energy Generating Systems

930   ST   Solar Tower

931   SWRO   sea water reverse osmosis

932   TCES   thermochemical energy storage

933   TES   thermal energy storage

934   TETR   Traditional External Tubular Receiver

935   VVR   Variable Velocity Receiver

936   **References**

937   [1] Romero-Alvarez, M. and Zarza, E., Concentrating solar thermal power. Handbook of energy efficiency and
938   renewable energy, 2007:21-1.

939   [2] Müller-Steinhagen, H. and Trieb, F., Concentrating solar power. A review of the technology. Ingenia Inform
940   QR Acad Eng, 2004, 18:43-50.

941   [3] Zhang, H.L., Baeyens, J., Degrève, J. and Cacères, G., Concentrated solar power plants: Review and design
942   methodology. Renewable and Sustainable Energy Reviews, 2013, 22:466-481.

943   [4] Barlev, D., Vidu, R. and Stroeve, P., Innovation in concentrated solar power. Solar Energy Materials and
944   Solar Cells, 2011, 95(10):2703-2725.

945   [5] Winter, C.J., Sizmann, R.L. and Vant-Hull, L.L. eds., 2012. Solar power plants: fundamentals, technology,
946   systems, economics. Springer Science & Business Media.

947   [6] Sawin, J.L. and Martinot, E., Renewables bounced back in 2010, finds REN21 global report. Renewable
948   Energy World, 2011, 14(5):29.
949   www.renewableenergyworld.com/articles/print/volume-14/issue-5/solar-energy/renewables-bounced-bac
950   k-in-2010-finds-ren21-global-report.html , Retrieved November 9, 2017.

951   [7] Renewable Energy Policy Network for the 21st Century (REN21), Renewables Global Status Report 2017,
952   2017. www.ren21.net/wp-content/uploads/2017/06/17-8399_GSR_2017_Full_Report_0621_Opt.pdf,
953   Retrieved November 8, 2017.

954   [8] Boretti, A., Concentrated Solar Power Plants Capacity Factors: A Review, Nonlinear Approaches in
955   Engineering Applications Energy: Vibrations, and Modern Applications, Liming Dai, Eds., Reza N. Jazar,
956   Springer, New York, 2017.

957   [9] Lilliestam, J., After the Desertec hype: is concentrating solar power still alive?, September 2017.
958   www.ethz.ch/en/news-and-events/eth-news/news/2017/09/concentrating-solar-power.html, Retrieved
959   November 9, 2017.

960   [10] International Energy Agency, 2016 Key world energy statistics, 2016.
961   www.iea.org/publications/freepublications/publication/KeyWorld2016.pdf, Retrieved November 8, 2017.

962   [11] Energy Information Administration, Electricity data browser – Net generation for all sectors – United
963   States.   www.eia.gov/electricity/data/browser, Retrieved November 9, 2017.

964   [12] National Renewable Energy Laboratory (NREL), Concentrating Solar Power Projects - Ivanpah Solar
965   Electric. www.nrel.gov/csp/solarpaces/project_detail.cfm/projectID=62, Retrieved November 8, 2017.

966   [13] Energy Information Administration, Electricity data browser – Plant Level Data Ivanpah 1.
967   www.eia.gov/electricity/data/browser/#/plant/57074/, Retrieved November 9, 2017.

968   [14] Energy Information Administration, Electricity data browser – Plant Level Data Ivanpah 2.
969   www.eia.gov/electricity/data/browser/#/plant/57073/, Retrieved November 9, 2017.

970   [15] Energy Information Administration, Electricity data browser – Plant Level Data Ivanpah 3.
971   www.eia.gov/electricity/data/browser/#/plant/57075/, Retrieved November 9, 2017.

[16] del Río, P., Peñasco, C. and Mir-Artigues, P., An overview of drivers and barriers to concentrated solar power in the European Union. Renewable and Sustainable Energy Reviews, 2018, 81:1019-1029.

[17] de Souza, L.E.V. and Cavalcante, A.M.G., Concentrated Solar Power deployment in emerging economies: The cases of China and Brazil. Renewable and Sustainable Energy Reviews, 2017, 72:1094-1103.

[18] National Renewable Energy Laboratory (NREL), Power Tower Projects, www.nrel.gov/csp/solarpaces/power_tower.cfm, Retrieved November 9, 2017.

[19] ABENGOA SOLAR, Concentrating Solar Power: State of the Art. ARPA-E Solar Beyond Grid Parity: Spectrum-Efficient Solar Energy for Dispatchable Electricity or Fuels Workshop, Boulder, CO April 11-12 2013. www.arpa-e.energy.gov/sites/default/files/documents/files/SolarBeyondGridParity_Erickson.pdf retrieved November 9, 2017.

[20] Margolis, R., Coggeshall, C. and Zuboy, J., SunShot vision study. US Dept. of Energy, 2012.

[21] Kearney, D. and Herrmann, U., *Engineering evaluation of a molten salt heat transfer fluid in a parabolic trough solar field*. National Renewal Energy Laboratoy, 2006.

[22] Feldhoff, J.F., Schmitz, K., Eck, M., Schnatbaum-Laumann, L., Laing, D., Ortiz-Vives, F. and Schulte-Fischedick, J., Comparative system analysis of direct steam generation and synthetic oil parabolic trough power plants with integrated thermal storage. Solar Energy, 2012, 86(1): 520-530.

[23] Bendt, P., Rabl, A., Gaul, H.W. and Reed, K.A., Optical analysis and optimization of line focus solar collectors (No. NREL/TR-34-92). National Renewable Energy Laboratory (NREL), Golden, CO, 1979.

[24] Reilly, H.E. and Kolb, G.J., An evaluation of molten-salt power towers including results of the solar two project (No. SAND2001-3674). Sandia National Labs., Albuquerque, NM (US); Sandia National Labs., Livermore, CA (US), 2007.

[25] Radosevich, L.G., Final Report on the Power Production Phase of the 10 MWe Solar Thermal Central Receiver Pilot Plant, SAND87-8022. Sandia National Laboratories, Albuquerque, NM, 1988.

[26] Thermoflow, Inc., "Thermoflow". www.thermoflow.com/, Retrieved November 9, 2017.

[27] National renewable Energy Laboratory, Concentrating Solar Power Projects by Project Name. www.nrel.gov/csp/solarpaces/by_project.cfm , Retrieved November 9, 2017.

[28] Energy Information Administration. Electricity data browser – Plant Level Data. www.eia.gov/electricity/data/browser/ , Retrieved November 9, 2017.

[29] Kuravi, S., Trahan, J., Goswami, D.Y., Rahman, M.M. and Stefanakos, E.K., Thermal energy storage technologies and systems for concentrating solar power plants. Progress in Energy and Combustion Science, 2013, 39(4):285-319.

[30] Sioshansi, R. and Denholm, P., The value of concentrating solar power and thermal energy storage. IEEE Transactions on Sustainable Energy, 2010, 1(3):173-183.

[31] Gil, A., Medrano, M., Martorell, I., Lázaro, A., Dolado, P., Zalba, B. and Cabeza, L.F., State of the art on high temperature thermal energy storage for power generation. Part 1—Concepts, materials and modellization. Renewable and Sustainable Energy Reviews, 2010, 14(1):31-55.

[32] Medrano, M., Gil, A., Martorell, I., Potau, X. and Cabeza, L.F., State of the art on high-temperature thermal energy storage for power generation. Part 2—Case studies. Renewable and Sustainable Energy Reviews, 2010, 14(1):56-72.

[33] Cavallaro, F., Fuzzy TOPSIS approach for assessing thermal-energy storage in concentrated solar power (CSP) systems. Applied Energy, 2010, 87(2):496-503.

[34] Price, H., Lupfert, E., Kearney, D., Zarza, E., Cohen, G., Gee, R. and Mahoney, R., Advances in parabolic trough solar power technology. Journal of solar energy engineering, 2002, 124(2):109-125.

1015 [35] National Renewable Energy Laboratory (NREL), Integrating Variable Renewable Energy Into the Grid.
1016   NREL/FS-6A20-63033, May 2015. www.nrel.gov/docs/fy15osti/63033.pdf , Retrieved November 9, 2017.
1017 [36] International Renewable Energy Agency (IRENA), Renewable Energy Integration in Power Grids. April
1018   2015.
1019   www.irena.org/DocumentDownloads/Publications/IRENA-ETSAP_Tech_Brief_Power_Grid_Integration_
1020   2015.pdf , Retrieved November 9, 2017.
1021 [37] American Physical Society, Integrating Renewable Electricity on the Grid. November 2011,
1022   www.aps.org/policy/reports/popa-reports/upload/integratingelec.pdf, Retrieved November 9, 2017.
1023 [38] Larson, A., World's Most-Efficient Combined Cycle Plant: EDF Bouchain, Power magazine, September 1,
1024   2017, www.powermag.com/worlds-most-efficient-combined-cycle-plant-edf-bouchain/ , retrieved
1025   November 9, 2017.
1026 [39] General Electric Company, POWERING A NEW RECORD AT EDF. 9HA.01 SETS EFFICIENCY WORLD
1027   RECORD, August 2016.
1028   www.gepower.com/content/dam/gepower-pgdp/global/en_US/documents/product/gas%20turbines/Whit
1029   e%20Paper/gea32885-bouchain-whitepaper-final-aug-2016.pdf, retrieved November 9, 2017.
1030 [40] Overton, T., Gas Combined Cycle Capacity Factors Beat Coal for First Time Ever, Power magazine,
1031   04/11/2016.www.powermag.com/gas-combined-cycle-capacity-factors-beat-coal-for-first-time-ever/,
1032   retrieved November 9, 2017.
1033 [41] Douglas, I., ISEGS Order Approving Petition to Amend, 15 September 2014.
1034   docketpublic.energy.ca.gov/PublicDocuments/07-AFC-05C/TN203064_20140915T132932_ISEGS_Order_A
1035   pproving_Petition_to_Amend.pdf, Retrieved November 9, 2017.
1036 [42] Danelski, D., It's not easy being green: Ivanpah solar plant near Nevada burns much natural gas, making it
1037   a greenhouse gas emitter under state law. Orange County Register. Santa Ana, California. 21 October 2015.
1038   www.ocregister.com/2015/10/21/its-not-easy-being-green-ivanpah-solar-plant-near-nevada-burns-a-lot-of
1039   -natural-gas-making-it-a-greenhouse-gas-emitter-under-state-law/, Retrieved November 9, 2017.
1040 [43] Price, H. and Kearney, D., Reducing the cost of energy from parabolic trough solar power plants. In
1041   International Solar Energy Conference. Hawaii Island, Hawaii, January 2003. National Renewable Energy
1042   Laboratory NREL/CP-550-33208.
1043 [44] National Renewable Energy Laboratory (NREL), Concentrating Solar Power Projects - Crescent Dunes
1044   Solar Energy, www.nrel.gov/csp/solarpaces/project_detail.cfm/projectID=60, Retrieved November 8, 2017.
1045 [45] Energy Information Administration, Electricity data browser – Plant Level Data Crescent Dunes Solar
1046   Energy,   www.eia.gov/electricity/data/browser/#/plant/57275/, Retrieved November 9, 2017.
1047 [46] Energy Information Administration (EIA), Construction cost data for electric generators installed in 2015.
1048   May 2017. www.eia.gov/electricity/generatorcosts/, retrieved November 9, 2017.
1049 [47] Energy Information Administration (EIA), Cost and Performance Characteristics of New
1050   GeneratingTechnologies, Annual Energy Outlook 2017. January 2017.
1051   www.eia.gov/outlooks/aeo/assumptions/pdf/table_8.2.pdf, retrieved November 9, 2017.
1052 [48] National Renewable Energy Laboratory (NREL), Concentrating Solar Power Projects - Solana Generating
1053   Station www.nrel.gov/csp/solarpaces/project_detail.cfm/projectID=23, Retrieved November 8, 2017.
1054 [49] Energy Information Administration, Electricity data browser – Plant Level Data Solana
1055   https://www.eia.gov/electricity/data/browser/#/plant/56812, Retrieved November 9, 2017.

1056 [50] National Renewable Energy Laboratory (NREL), Concentrating Solar Power Projects – Solar Electric
1057   Generating Station IX.   www.nrel.gov/csp/solarpaces/project_detail.cfm/projectID=36, Retrieved
1058   November 8, 2017.

1059 [51] Energy Information Administration, Electricity data browser – Plant Level Data SEGS IX
1060   www.eia.gov/electricity/data/browser/#/plant/10446/, Retrieved November 9, 2017.

1061 [52] Pfenninger, S., Gauché, P., Lilliestam, J., Damerau, K., Wagner, F. and Patt, A., Potential for concentrating
1062   solar power to provide baseload and dispatchable power. Nature Climate Change, 2014, 4(8):689-692.

1063 [53] Lilliestam J, Labordena M, Patt A, & Pfenninger S., Empirically observed learning rates for concentrating
1064   solar power and their responses to regime change. Nature Energy, 2017, 2:17094.

1065 [54] Srilakshmi, G., Venkatesh, V., Thirumalai, N.C. and Suresh, N.S., Challenges and opportunities for Solar
1066   Tower technology in India. Renewable and Sustainable Energy Reviews, 2015, 45:698-709.

1067 [55] Hoffschmidt, B., Receivers for Solar Tower Systems. CNRS 2014 SFERA School, June 25-27, 2014, Font
1068   Romeu, France. elib.dlr.de/94540/1/SFERA2014_SolarTowerReceivers_final.pdf, Retrieved November 9,
1069   2017.

1070 [56] Vignarooban, K., Xu, X., Arvay, A., Hsu, K. and Kannan, A.M., Heat transfer fluids for concentrating solar
1071   power systems–a review. Applied Energy, 2015, 146:383-396.

1072 [57] Liu, M., Belusko, M., Tay, N.S. and Bruno, F., Impact of the heat transfer fluid in a flat plate phase change
1073   thermal storage unit for concentrated solar tower plants. Solar Energy, 2014, 101:220-231.

1074 [58] Pelay, U., Luo, L., Fan, Y., Stitou, D. and Rood, M., Thermal energy storage systems for concentrated solar
1075   power plants. Renewable and Sustainable Energy Reviews, 2017, 79:82-100.

1076 [59] González-Roubaud, E., Pérez-Osorio, D. and Prieto, C., Review of commercial thermal energy storage in
1077   concentrated solar power plants: Steam vs. molten salts. Renewable and Sustainable Energy Reviews,
1078   2017, 80:133-148.

1079 [60] Zhang, H., Benoit, H., Perez-Lopèz, I., Flamant, G., Tan, T. and Baeyens, J., High-efficiency solar power
1080   towers using particle suspensions as heat carrier in the receiver and in the thermal energy storage.
1081   Renewable Energy. 2017.

1082 [61] Alexopoulos, S. and Hoffschmidt, B., Advances in solar tower technology. Wiley Interdisciplinary Reviews:
1083   Energy and Environment, 2017, 6(1).

1084 [62] Peng, X., Root, T.W. and Maravelias, C.T., Storing solar energy with chemistry: the role of thermochemical
1085   storage in concentrating solar power. Green Chemistry, 2017, 19(10):2427-2438.

1086 [63] Tescari, S., Singh, A., Agrafiotis, C., de Oliveira, L., Breuer, S., Schlögl-Knothe, B., Roeb, M. and Sattler, C.,
1087   Experimental evaluation of a pilot-scale thermochemical storage system for a concentrated solar power
1088   plant. Applied Energy, 2017, 189:66-75.

1089 [64] Pacheco, J.E., Wolf, T. and Muley, N., Incorporating Supercritical Steam Turbines Into Advanced
1090   Molten-Salt Power Tower Plants: Feasibility and Performance. Sandia National Laboratories,
1091   Albuquerque, NM, Report No. SAN2013-1960, 2013.

1092 [65] Turchi, C.S., Ma, Z., Neises, T.W. and Wagner, M.J., Thermodynamic study of advanced supercritical
1093   carbon dioxide power cycles for concentrating solar power systems. Journal of Solar Energy Engineering,
1094   2013, 135(4):041007.

1095 [66] Zheng, H., Yu, X., Su, Y., Riffat, S. and Xiong, J., Thermodynamic analysis of an idealised solar tower
1096   thermal power plant. Applied Thermal Engineering, 2015, 81:271-278.

1097 [67] Schmitt, J., Wilkes, J., Allison, T., Bennett, J., Wygant, K. and Pelton, R., Lowering the Levelized Cost of
1098   Electricity of a Concentrating Solar Power Tower with a Supercritical Carbon Dioxide Power Cycle. In

1099   ASME Turbo Expo 2017: Turbomachinery Technical Conference and Exposition (pp.

1100   V009T38A028-V009T38A028). American Society of Mechanical Engineers, 2017, June.

1101   [68] Stein, W.H. and Buck, R., Advanced power cycles for concentrated solar power. Solar Energy, 2017,

1102   152:91-105.

1103   [69] Binotti, M., Astolfi, M., Campanari, S., Manzolini, G. and Silva, P., Preliminary assessment of sCO 2 cycles

1104   for power generation in CSP solar tower plants. Applied Energy.

1105   [70] Wang, K., He, Y.L. and Zhu, H.H., Integration between supercritical CO 2 Brayton cycles and molten salt

1106   solar power towers: A review and a comprehensive comparison of different cycle layouts. Applied

1107   Energy, 2017, 195:819-836.

1108   [71] Rodríguez-Sánchez, M.R., Sánchez-González, A., González-Gómez, P.A., Marugán-Cruz, C. and Santana,

1109   D., Thermodynamic and economic assessment of a new generation of subcritical and supercritical solar

1110   power towers. Energy, 2017, 118:534-544.

1111   [72] Atif, M. and Al-Sulaiman, F.A., Energy and exergy analyses of solar tower power plant driven supercritical

1112   carbon dioxide recompression cycles for six different locations. Renewable and Sustainable Energy

1113   Reviews, 2017, 68:153-167.

1114   [73] Poživil, P. and Steinfeld, A., Integration of a Pressurized-Air Solar Receiver Array to a Gas Turbine Power

1115   Cycle for Solar Tower Applications. Journal of Solar Energy Engineering, 2017, 139(4), p.041007.

1116   [74] Ho, C.K. and Iverson, B.D., Review of high-temperature central receiver designs for concentrating solar

1117   power. Renewable and Sustainable Energy Reviews, 2014, 29:835-846.

1118   [75] Rodríguez-Sánchez, M.R., Sánchez-González, A. and Santana, D., Feasibility study of a new concept of

1119   solar external receiver: variable velocity receiver. Applied Thermal Engineering. 2018. 128:335-344.

1120   [76] Salomé, A., Chhel, F., Flamant, G., Ferrière, A. and Thiery, F., Control of the flux distribution on a solar

1121   tower receiver using an optimized aiming point strategy: Application to THEMIS solar tower. Solar

1122   Energy, 2013, 94:352-366.

1123   [77] Carrizosa, E., Domínguez-Bravo, C.A., Fernández-Cara, E. and Quero, M., An optimization tool to design

1124   the field of a solar power tower plant allowing heliostats of different sizes. International Journal of Energy

1125   Research. 2017.

1126   [78] Roldán, M.I., Fernández-Reche, J. and Ballestrín, J., Computational fluid dynamics evaluation of the

1127   operating conditions for a volumetric receiver installed in a solar tower. Energy, 2016, 94:844-856.

1128   [79] Hoffschmidt, B., Tellez, F.M., Valverde, A., Fernández, J. and Fernández, V., Performance evaluation of the

1129   200-kWth HiTRec-II open volumetric air receiver, 2003. Journal of Solar Energy Engineering, 125(1):87-94.

1130   [80] He, Y.L., Cui, F.Q., Cheng, Z.D., Li, Z.Y. and Tao, W.Q., Numerical simulation of solar radiation

1131   transmission process for the solar tower power plant: from the heliostat field to the pressurized volumetric

1132   receiver. Applied Thermal Engineering, 2013, 61(2):583-595.

1133   [81] Luo, Y., Du, X. and Wen, D., Novel design of central dual-receiver for solar power tower. Applied Thermal

1134   Engineering, 2015, 91:1071-1081.

1135   [82] Qiu, Y., He, Y.L., Li, P. and Du, B.C., A comprehensive model for analysis of real-time optical performance

1136   of a solar power tower with a multi-tube cavity receiver. Applied Energy, 2017, 185:589-603.

1137   [83] Thalange, V.C., Dalvi, V.H., Mahajani, S.M., Panse, S.V., Joshi, J.B. and Patil, R.N., Design, optimization and

1138   optical performance study of tripod heliostat for solar power tower plant. Energy, 2017, 135:610-624.

1139   [84] Deng, Q., Xiao, X., Hao, Y., Wang, Q., Hu, T. and Wang, Y., Heat transfer performance evaluation of a

1140   large-size cavity receiver in the solar power tower plant based on angle factors. Solar Energy, 2017,

1141   148:78-86.

[85] Fleming, A., Folsom, C., Ban, H. and Ma, Z., 2017. A general method to analyze the thermal performance of multi-cavity concentrating solar power receivers. Solar Energy, 2017, 150:608-618.

[86] Hischier, I., Poživil, P. and Steinfeld, A., Optical and Thermal Analysis of a Pressurized-Air Receiver Cluster for a 50 MWe Solar Power Tower. Journal of Solar Energy Engineering, 2015, 137(6), p.061002.

[87] Li, X., Lin, M., Dai, Y. and Wang, C.H., Comparison-based optical assessment of hyperboloid and ellipsoid reflectors in a beam-down solar tower system with linear Fresnel heliostats. Journal of Solar Energy Engineering, 2017, 139(6):061003.

[88] Pabst, C., Feckler, G., Schmitz, S., Smirnova, O., Capuano, R., Hirth, P. and Fend, T., Experimental performance of an advanced metal volumetric air receiver for Solar Towers. Renewable Energy, 2017, 106:91-98.

[89] López-Herraiz, M., Fernández, A.B., Martinez, N. and Gallas, M., Effect of the optical properties of the coating of a concentrated solar power central receiver on its thermal efficiency. Solar Energy Materials and Solar Cells, 2017, 159:66-72.

[90] Boubault, A., Ho, C.K., Hall, A., Lambert, T.N. and Ambrosini, A., Durability of solar absorber coatings and their cost-effectiveness. Solar Energy Materials and Solar Cells, 2017, 166:176-184.

[91] Rodríguez-Palomo, A., Céspedes, E., Hernández-Pinilla, D. and Prieto, C., High-temperature air-stable solar selective coating based on MoSi 2–Si 3 N 4 composite. Solar Energy Materials and Solar Cells, 2018, 174:50-55.

[92] Okoroigwe, E. and Madhlopa, A., An integrated combined cycle system driven by a solar tower: A review. Renewable and Sustainable Energy Reviews, 2016, 57:337-350.

[93] Franchini, G., Perdichizzi, A., Ravelli, S. and Barigozzi, G., A comparative study between parabolic trough and solar tower technologies in Solar Rankine Cycle and Integrated Solar Combined Cycle plants. Solar Energy, 2013, 98:302-314.

[94] Zachary, J. and Layman, C.M., 2010. Adding Desalination to Solar Hybrid and Fossil Plants. Power, 154(5).

[95] Trieb, F. and Müller-Steinhagen, H., 2008. Concentrating solar power for seawater desalination in the Middle East and North Africa. Desalination, 220(1-3):165-183.

[96] Demir, M.E. and Dincer, I., Development and analysis of a new integrated solar energy system with thermal storage for fresh water and power production. International Journal of Energy Research. 2017, DOI: 10.1002/er.3846.

[97] Kumar, A., Prakash, O. and Dube, A., A review on progress of concentrated solar power in India. Renewable and Sustainable Energy Reviews, 2017, 79:304-307.

[98] Abu-Hamdeh, N.H. and Alnefaie, K.A., Design considerations and construction of an experimental prototype of concentrating solar power tower system in Saudi Arabia. Energy Conversion and Management, 2016, 117:63-73.

[99] Amadei, C.A., Allesina, G., Tartarini, P. and Yuting, W., Simulation of GEMASOLAR-based solar tower plants for the Chinese energy market: Influence of plant downsizing and location change. Renewable energy, 2013, 55:366-373.

[100] Yamani, N., Khellaf, A., Mohammedi, K. and Behar, O., Assessment of solar thermal tower technology under Algerian climate. Energy, 2017, 126:444-460.

[101] US Inflation Calculator, www.usinflationcalculator.com/, Retrieved November 9, 2017.

[102] Williges, K., Lilliestam, J. & Patt, A. Making concentrated solar power competitive with coal: the costs of a European feed-in tariff. Energy Policy, 2010, 38:3089–3097.

1184   [103] Neij, L. Cost development of future technologies for power generation - A study based on experience

1185   curves and complementary bottom-up assessments. Energy Policy, 2008, 36:2200–2211.

1186   [104] Viehbahn, P., Lechon, Y. & Trieb, F. The potential role of concentrated solar power (CSP) in Africa and

1187   Europe. Energy Policy, 2011, 39, 4420–4430.